DESIGN OF COMPLEMENTARY EXPERIMENTS FOR ESTIMATION OF TEMPERATURE-DEPENDENT THERMAL PROPERTIES

by

Halak Mehta

A Thesis

Submitted to the Faculty of Purdue University

In Partial Fulfillment of the Requirements for the degree of

Master of Science

Department of Food Science

West Lafayette, Indiana

May 2020

THE PURDUE UNIVERSITY GRADUATE SCHOOL
STATEMENT OF COMMITTEE APPROVAL

Dr. Dharmendra K. Mishra, Chair

Department of Food Science

Dr. Carlos Corvalan

Department of Food Science

Dr. Michael Varney

Chief Technical Officer, Thermetrics, Inc.

Approved by:

Dr. Arun Bhunia

Dedicated to my parents, for being my steadfast pillars of strength, guidance, encouragement and belief

ACKNOWLEDGMENTS

I would like to express my utmost gratitude to Dr. Dharmendra Mishra, for his many many lessons to me. Under his mentorship, I have received plethora of opportunities to grow as a researcher, an engineer, a leader and presenter. I have grown professionally and personally, and I am thankful to have gotten the chance to work with him. He has been a great source of inspiration, insight and advice.

I would like to extend my heartfelt thanks to my committee members, Dr. Carlos Corvalan and Dr. Michael Varney for their exceptional inputs, guidance and support. I would also like to thank Dr. James Beck and Dr. Kirk Dolan for their contribution and giving me the incredible opportunity to learn from them. I would like to acknowledge the NSF foundation and the STTR grant (Award #1722154).

I would be remiss without the mention of the Mishra lab group. The lab group has made the past few years a fun journey. Working, learning and growing with them has been a wonderful experience. Special mention to Rhonda Taylor, for making sure I never missed home and being an amazing friend.

My friends and family have been my source of joy, and I consider myself blessed to have them in my life. I am very thankful for their well-wishes and advice. Lastly, I would like to thank my parents for all they have done throughout the years.

TABLE OF CONTENTS

LIST OF TABLES

LIST OF FIGURES

LIST OF SYMBOLS

α_h	Thermal diffusivity of thin film heater, m^2/s
C	Volumetric heat capacity, J/m^3K
C_a	Volumetric heat capacity of air, J/m^3K
C_h	Volumetric heat capacity of thin film heater, J/m^3K
C_s	Volumetric heat capacity of stainless steel, J/m^3K
C_1	Volumetric heat capacity at temperature T_1, J/m^3K
C_2	Volumetric heat capacity at temperature T_2, J/m^3K
h	Convective heat transfer coefficient, W/m^2K
k	Thermal conductivity, W/mK
k_a	Thermal conductivity of air, W/mK
k_h	Thermal conductivity of thin film heater, W/mK
k_s	Thermal conductivity of stainless steel, W/mK
k_1	Thermal conductivity at temperature T_1, W/mK
k_2	Thermal conductivity at temperature T_2, W/mK
n	Number of measurements
p	Number of parameters
r	Position along radial direction, in
t	Time, s
T	Temperature, ℃
T_0	Initial temperature, ℃
T_1	Initial reference temperature for thermal properties, ℃
T_2	Final reference temperature for thermal properties, ℃
X	Sensitivity Matrix, ℃/[parameter units]

ABSTRACT

Thermal processing is a critical step in shelf-stable food manufacturing to the ensure safety of the food products. To accurately model and establish the thermal processes, temperature-dependent thermal properties are needed. Existing methods for measuring the temperature-dependent thermal diffusivity (α), thermal conductivity (k) and volumetric heat capacity (C) are time consuming, tend to have high errors, and cannot provide results in a single experiment, especially at temperatures above 100°C. A novel bench scale device, named Thermal Properties Cell (TPCell), was custom made to rapidly estimate the temperature-dependent thermal parameters of food products.

The TPCell used thin film heaters as the heating elements. The first study focused on estimating the thermal properties of a thin film heater. Using mathematical modeling and sequential parameter estimation, the effective thermal diffusivity of the thin film heater was found at different temperatures. The estimated thermal properties of the thin film heater were used for the second study.

The objective of the second study was to design optimal complementary experiments using TPCell. Complementary experiments are a combination of experiments that enable estimation of multiple thermal parameters from the experimental temperature data, based on sensitivity analysis. Sensitivity coefficients indicate the extent of change in a measured variable due to a change in value of an input parameter. Designs of experiments were simulated and their impact on sensitivity and optimality criteria was analyzed. Results from the simulated profiles were validated using sweet potato puree.

Learnings from this work can be directly applied for the optimization of all types of food thermal processes, including retort and aseptic processing. Optimally designed processes increase preservation of the heat labile nutrients, color, flavor, and taste compounds, thereby enhancing the quality of food products.

CHAPTER 1. ESTIMATION OF EFFECTIVE THERMAL DIFFUSIVITY OF THIN FILM HEATER USING INVERSE METHODS

1.1 Abstract

Characterization of heating source is important to predict its performance for various applications and especially in a sensor design. A thin film heater, made of layers of polyimide and Monel, was selected. A Nickel resistance temperature detector (RTD) was embedded in the heater to record temperature change. The thin film heater was calibrated using an oil bath. After calibration, the thermal response of the heater to external heat flux was recorded using the embedded RTD. A one-dimensional radial axisymmetric heat transfer model was created for the parameter estimation. Sensitivity analysis was performed to determine number of parameters that can be estimated from the temperature measurements. It was found that with a convective boundary condition, thermal conductivity and volumetric specific heat cannot be estimated simultaneously. However, a combination the parameters, the thermal diffusivity, can be estimated. Sequential method of parameter estimation was used to estimate the thermal diffusivity of thin film heater. The precision and errors around the estimates were calculated. The effective thermal diffusivity was found to be 4.5×10^{-9} m^2/s, $1.039 \times 10^{-8} m^2/s$, 1.04×10^{-8} m^2/s at 105°C, 115°C, and 125°C respectively. The estimated values closely matched values in published literature. Thermal properties of the heater were found to be dependent on temperature. The thin film heater was used as a component in the experimental assembly to measure thermal properties of food materials at elevated temperatures.

1.2 Introduction

Heat transfer within a material depends on its physical, thermal and flow properties. Rate of heat transfer in a system is impacted by characteristics such as state, shape, size, porosity, thermal conductivity, specific heat capacity, density, viscosity and ambient temperature (Incropera et. al, 2007). The heating source plays a crucial role in the efficacy of heat transfer. The heating source is controlled to provide a fixed amount of heat to the medium for a fixed amount of time. The

design and characterization of the heat source are critical for the manufacturing of an efficient heating system.

Electric heaters are frequently used for industrial and research applications. Electric heaters convert electrical energy into thermal energy. While there are many kinds of electric heaters available, this study is focused on thin film heaters. Thin film heaters have been used increasingly in applications ranging from microelectronics to biotechnology (Golan et. al, 2003). An ideal heater should have quick heating response, uniform heat distribution, durability, high tensile strength and corrosion resistance. For some applications, the heaters also have temperature sensors embedded in the body of the heater. Temperature sensors should be robust and cost-effective, with high sensitivity and wide temperature range (Neitzert et. al, 2011). To characterize thermal behavior of a heater, it is essential to know its thermal properties.

Methods of measurement of thermal properties can be broadly divided into two categories: steady state and transient state. In steady state methods, thermal properties are measured when the sample attains thermal equilibrium with the heating medium. These measurements are time consuming and require extensive sample preparation (Herzen et. al, 1959).

Transient methods of measurements are faster and applicable over a wide range of temperatures. Two types of transient methods are among the most popular: transient line source and transient plane source. Transient line source, also called the transient hot wire method, typically consists of a small probe inserted in a small solid sample. A thermocouple and hot-wire are placed inside the probe (Sweat and Haugh, 1974). The heating of the hot-wire causes a change in the temperature of the sample surrounding the probe. This change in temperature, measured by the thermocouple, is used to calculate the thermal conductivity of the sample.

The transient plane source theory and device originated in the work of Gustafsson (1991). A square or disk-shaped temperature sensor is sandwiched between two identical samples (Hang and Liu, 2009, Ahadi et. al, 2016). The temperature sensor acts as a heat source and temperature indicator. An electric current is applied to the sensor, resulting in increased thermal energy of the sensor.

This increase in temperature causes a temperature change in samples placed on either side, which can be correlated with the thermal properties of the sample.

Inverse methods are a powerful tool to determine thermal properties. Inverse methods have been used to estimate the thermal properties of materials ranging from cherry pomace to steel slabs, biological tissue to reinforced epoxy composites (Greiby et. al, 2014; Telejko, 2004; Huang and Huang, 2007; Saad et. al, 2014). The inverse problem approach consists of estimating parameters (constants in a model) from response data. In the inverse problem discussed in this study, the temperature was the response variable and thermal properties were the parameters to be estimated. The feasibility of estimating a parameter accurately from temperature data depends on the sensitivity coefficients of the parameters. Sensitivity coefficients measure the extent of change in a measured variable due to a small change in the value of an input parameter. Scaled sensitivity coefficients are sensitivity coefficients multiplied by the parameter value. Scaled sensitivity coefficients should be large and uncorrelated to accurately and simultaneously estimate multiple parameters (Beck and Arnold, 1977).

A lack of research was found for determining the thermal properties of a heat source. In the literature reviewed, only one study estimated thermal properties of a mica heater using parameter estimation (Dowding, 1995). Dowding et. al emphasize the significance and unavailability of data on heater thermal properties (Dowding, 1999).

The objective of this study was to estimate the effective thermal diffusivity of a thin film heater using inverse methods.

1.3 Materials and Methods

1.3.1 Heater Details and Experimental Setup

The thin film heater was a hollow cylinder, 0.235” ID x 0.25” OD x 6” length in dimensions. The heater was made of several layers. The outermost layer was made of aluminum to increase rigidity. Two layers of polyimide were used to provide electrical insulation. A Monel layer, used as a heat source, was sandwiched between the polyimide layers. The layers were bound together using bond

ply. A Resistance Temperature Detector (RTD), made of Nickel 201, was embedded in a 0.25” x 1.5” area around the center of the heater. The total thickness of the heater was 0.015”. Fig. 1.1 shows the arrangement of heater layers in the central area of the heater.

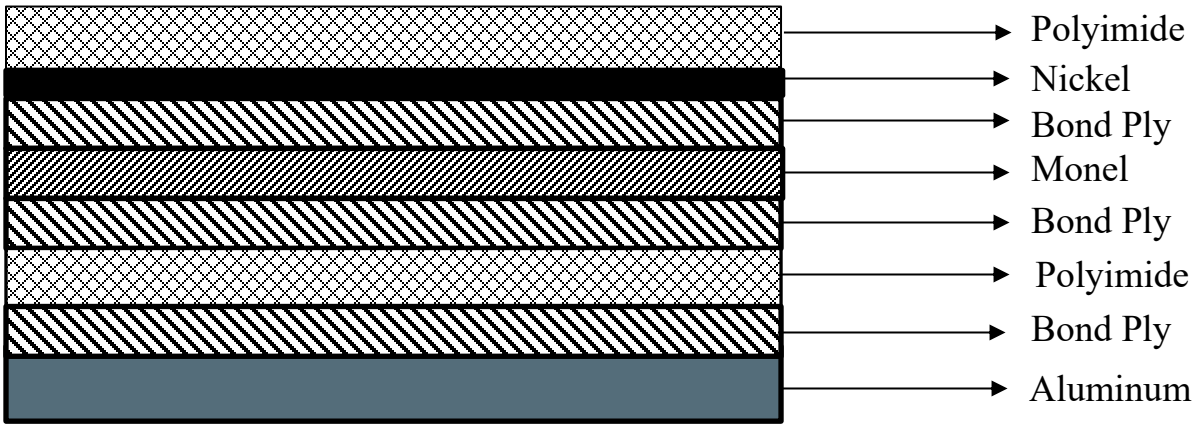

Figure 1.1 Layers of the thin film heater

The thickness of each layer, as provided by the manufacturer, is listed in Table 1.1. It was not possible to verify the thickness of the individual layers.

Table 1.1 Thickness of each layer in the thin film heater

Layer	Thickness (in)
Aluminum	0.003
Bond ply	0.002
Monel	0.002
Nickel	0.001
Polyimide	0.0025

The heater had a maximum power rating of 150 W and maximum temperature rating of 150°C.

Figure 1.2 Thin Film Heater

The heater was connected to a bench scale control system consisting of the following components:

1. PSB24-240S Power supply (AutomationDirect.com, Cumming, Georgia) – A 24V VDC output power supply, mounted on 35 mm rails, provided DC power to the control circuit.
2. PSB48-240S Power supply (AutomationDirect.com, Cumming, Georgia) – A 48V VDC output power supply, mounted on 35 mm rails, used in conjunction with PSB24-240s, provided DC power to the control circuit.
3. EK1100 EtherCAT Coupler (Beckhoff Automation GmbH & Co. KG, Verl, Germany) – The EK1100 coupler was used as a connector between the EtherCAT terminals (the EL series) and the PC. The EK1100 had ethernet ports to connect to the PC via an ethernet cable to transmit data and signals to and from the circuit.
4. EL7342 2-channel DC motor output stage 50 V DC, 3.5 A (Beckhoff Automation GmbH & Co. KG, Verl, Germany) – The EL7342 enabled use of the two DC motors to provide DC to the circuit. The power supply to the heater was regulated through the EL7342.

5. EL3312 2-channel thermocouple input terminal with open-circuit recognition (Beckhoff Automation GmbH & Co. KG, Verl, Germany) – The EL3312 was used to connect and transmit temperature data from thermocouples. Two J-type thermocouples were connected to the EL 3312 to record ambient temperature.
6. EL3202 2-channel input terminal PT100 (RTD) for 3-wire connection (Beckhoff Automation GmbH & Co. KG, Verl, Germany) – The EL3202 was used to measure temperature reading of the RTD sensors. The initial resistance of the RTD at a reference temperature (usually room temperature) is used as a base value for conversion of resistance to temperature. The equations for conversion are coded as a part of the PLC software. The RTD is also referenced to a calibrated J-type thermocouple for the initial temperature. The accuracy of the thermocouple temperature impacts accuracy of the RTD readings.
7. FAZ-C4-1-NA and FAZ-C10-1-NA miniature circuit breakers (Eaton Corporation Inc, Dublin, Ireland) – The two circuit breakers, rated for 4 A and 10 A respectively, were used as safety switches. In case of a short circuit, the circuit breakers would curtail excessive currents and prevent damage to the system.
8. Software Interface – The PLC software, based in TwinCAT 3, was custom made for control and data acquisition. In addition, a custom programmable user interface software was developed to interface with the PLC and save test data.

1.3.2 Temperature Calibration

Temperature data from the RTD was compared to data from a calibrated J-type thermocouple to verify the accuracy of the RTD readings. Using a calibration bath with silicone oil, the RTD temperature was recorded for bath set points ranging from 35°C to 135°C, at 10°C intervals. The calibration of the RTD was found to be non-linear. However, it was found that the relationship between RTD temperature and actual temperature remained linear for 10°C intervals. Hence, the RTD was calibrated in a step-wise fashion with 10°C steps, except for the first step, which ranges from room temperature to 45°C. The following equations were obtained for calibration:

Table 1.2 Calibration equations for RTD at 10°C steps

RTD Temperature (x)	Calibration Equation
Room Temperature - 45°C	0.9901x + 0.1485
45°C - 55°C	0.9804x + 0.5882
55°C - 65°C	0.9524x + 2.1429
65°C - 75°C	0.9346x + 3.3178
75°C - 85°C	0.885x + 7.1239
85°C - 95°C	0.8929x + 6.4286
95°C - 105°C	0.8621x + 9.4828
105°C - 115°C	0.8547x + 10.299
115°C - 125°C	0.8197x + 14.59
125°C - 135°C	0.7937x + 18.095

1.3.3 Design of Experiment

In the first set of experiments, the heater was immersed in an oil bath maintained at 105°C. Before the start of the experiment, the heater was at room temperature. The bath was heated to 105°C. Once the bath was ready, at time t = 0, the heater was dropped in the bath. RTD temperature was recorded continuously for 200 seconds. RTD temperature rose quickly from room temperature and stabilized as thermal equilibrium was achieved with the oil bath. The thermal behavior of the heater in the presence of an external heat source was used to estimate the thermal diffusivity of the heater. Heat input from the oil bath was modeled as a convective boundary condition in COMSOL Multiphysics, an interactive simulation software based on finite element method, with heat transfer coefficient (h) = 1800 $W/m^2.K$ (Zohuri, 2017). The experiments were repeated for 115°C and 125°C. A triplicate set of data was obtained at each temperature.

1.3.4 Mathematical Model and Scaled Sensitivity Coefficients

The system was described by the following set of 1D axisymmetric heat transfer equations:

$$\frac{1}{r}\frac{\partial}{\partial r}\left[k_h r\frac{\partial T}{\partial r}\right]+g_0 f(t)=C_h\frac{\partial T}{\partial t}\ for\ R_0<r\le R_1,\ t>0 \quad \textbf{(1)}$$

where k_h and C_h were the thermal conductivity and volumetric heat capacity of the thin film heater, R_0 and R_1 were the inner and outer diameters of the hollow cylinder, respectively.

The initial condition was:

$$T(r,0)=T_0 \quad \textbf{(2)}$$

The boundary conditions were:

$$\text{At } r=R_0 \text{ and } r=R_1,\ -k\frac{dT}{dr}=h(T_{inf}-T) \quad \textbf{(3)}$$

where T_{inf} was the temperature of infinite fluid (silicone oil) surrounding the heater, h was the convective heat transfer coefficient of oil in oil bath.

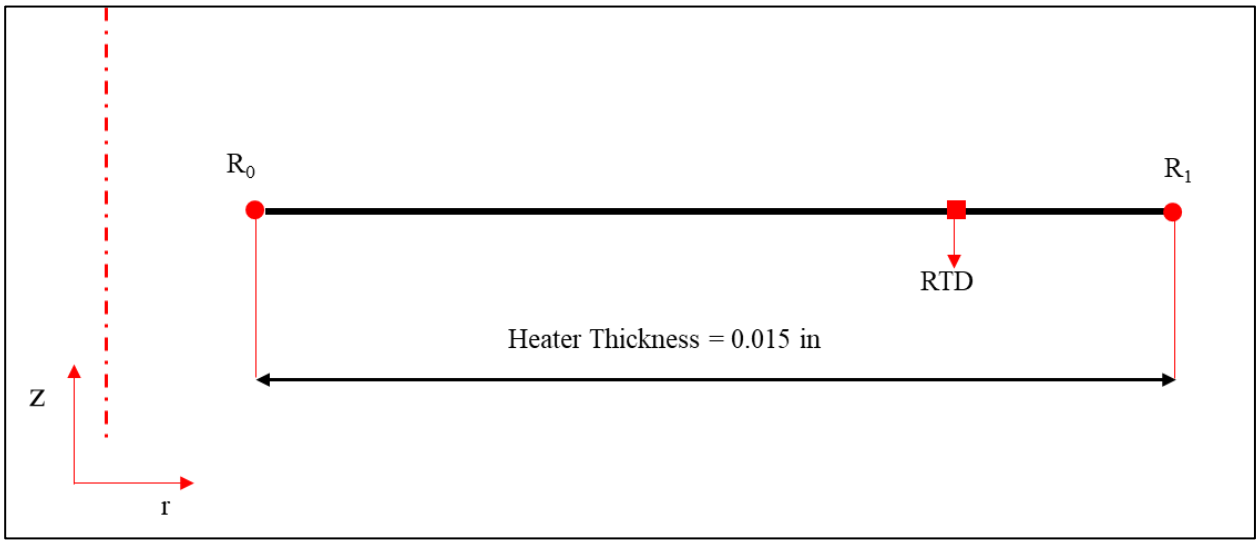

Figure 1.3 Schematic of 1D model of heater in COMSOL Multiphysics

As shown in Fig. 1.3, the heater was modeled and solved as a 1D axisymmetric model in COMSOL Multiphysics (COMSOL). The heater was modeled as a lumped body. Other models were also explored in which the heater was analyzed layer-wise. However, due to lack of verification of layer thickness, the lumped model was chosen. Verification of layers and respective thicknesses within the heater was not possible using any macro-level methods,

Initial values for parameter estimation of heater thermal properties were assumed. Thermal conductivity was assumed to be 0.01 W/mK and volumetric heat capacity was assumed as 2.4 x 10^6 J/m^3K. Heat transfer conditions identical to the experiments were provided to the model, and the temperature-time profile predicted by COMSOL was compared to experimental data.

Scaled sensitivity coefficients were calculated for k_h and C_h at each time point using equations shown below:

$$\hat{X}_{k_h} = k_h \frac{\partial T}{\partial k_h} \quad \textbf{(4)}$$

$$\hat{X}_{C_h} = C_h \frac{\partial T}{\partial C_h} \quad \textbf{(5)}$$

1.3.5 Sequential Estimation

Assuming all other variables in the model are known, the parameters to be determined were k_h and C_h. The difference between temperature predicted by the heat transfer model and the experimental temperature was minimized to obtain the parameters. The minimization function, based on the Gauss-Newton method, can be written in the matrix form as shown in Eq. 6:

$$S = \left[Y - \hat{Y}(\beta)\right]^T W \left[Y - \hat{Y}(\beta)\right] + \left[\mu - \beta\right]^T U \left[\mu - \beta\right] \quad \textbf{(6)}$$

where S denotes the sum of squares function, Y is the experimental data point, $\hat{Y}(\beta)$ is the predicted data point, β is the parameter vector, μ is prior information of β, W and U are symmetric weighting matrices, where U is inverse of the covariance matrix of parameters, and W is inverse of the covariance matrix of errors.

Sequential estimation iteratively minimizes the sum of square function at each time point and updates the value of the parameter in each iteration (Beck & Arnold, 1977). Based on matrix inversion lemma, the scheme of sequential estimation follows the below order (Eq. 7-12):

$$A(i+1) = P(i)\, X^T(i+1) \quad \textbf{(7)}$$

$$\Delta(i+1) = \Phi(i+1) + X(i+1)\, A(i+1) \quad \textbf{(8)}$$

$$K(i+1) = P(i)\,X^T(i+1)\,\Delta^{-1}(i+1) \quad \textbf{(9)}$$

$$b^*(i+1) = b^*(i) + K(i+1)\left\{e(i+1) - X(i+1)\left[b^*(i) - b\right]\right\} \quad \textbf{(10)}$$

$$P(i+1) = P(i) - K(i+1)\,X(i+1)\,P(i) \quad \textbf{(11)}$$

$$e(i+1) = Y(i+1) - \hat{Y}(i+1) \quad \textbf{(12)}$$

In the above set of equations, ***P*** represents the covariance matrix of parameters, ***X*** denotes the scaled sensitivity coefficient matrix, $\boldsymbol{b}^*(i+1)$ is the estimated parameter vector at the $(i+1)^{th}$ time point, $\boldsymbol{b}^*(i)$ is the estimated parameter vector at the i^{th} time point, ***b*** is the parameter vector at the end of previous iteration, ***e*** is the error vector, ***Y*** is the experimental data point, $\hat{\boldsymbol{Y}}$ is the predicted data point, **Φ** is the matrix of variance of errors in ***Y*.**

1.4 Results and Discussion

1.4.1 Temperature Calibration

The RTD embedded in the heater was calibrated according to the equations listed in Table 1 in the previous section. Fig. 1.4 shows temperature data as recorded by the RTD before calibration. The bath temperature was maintained at 125°C. No power was supplied to the heater. As seen in the plot, the RTD temperature was 9.2°C higher than the true temperature at the maximum. Fig. 1.5 depicts RTD data after calibration.

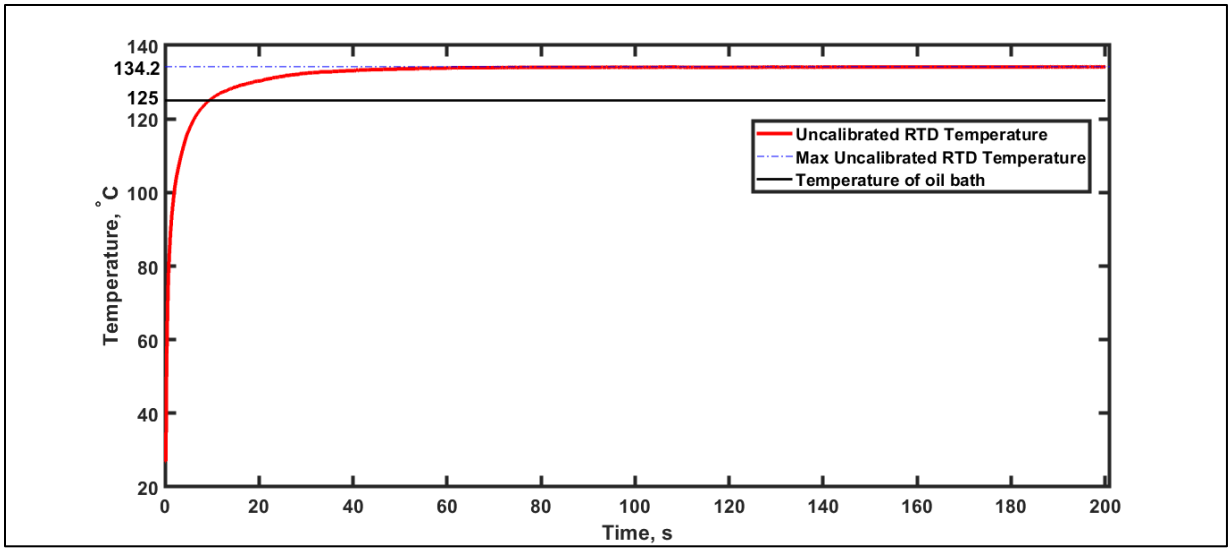

Figure 1.4 Uncalibrated RTD Temperature for oil bath temperature 125°C

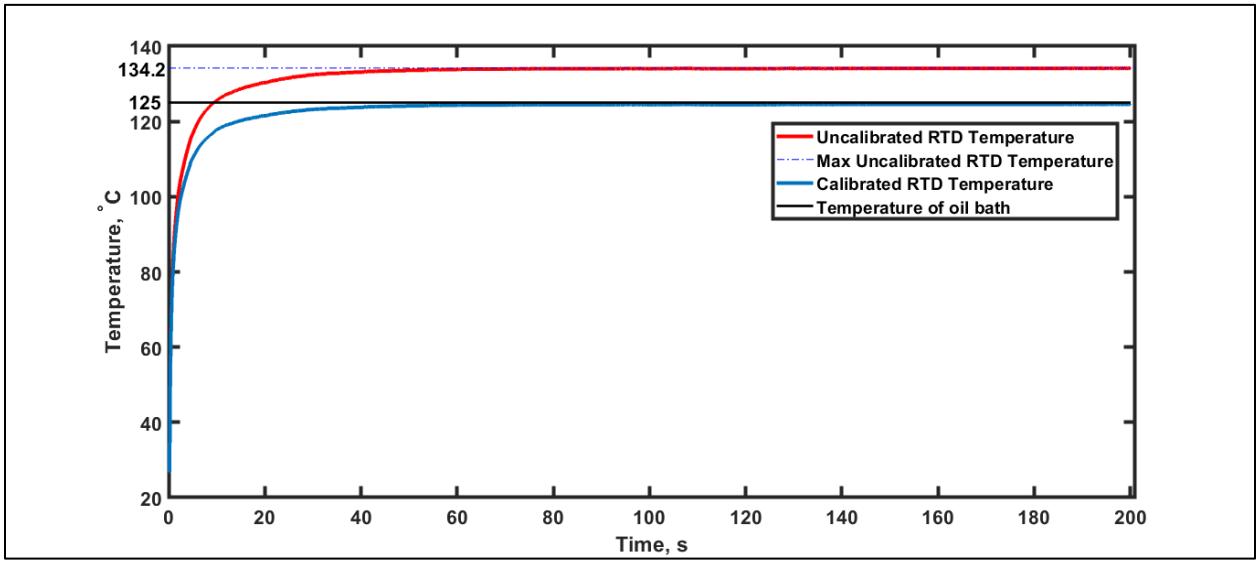

Figure 1.5 RTD Temperature after step-wise correction

1.4.2 Data Smoothing

The experimental data acquisition was discrete with a sampling interval of 0.01 s. The predicted temperature, on the other hand, was continuous. It was observed that the non-continuous recording of the RTD temperature resulted in an increased difference between the two, leading to high errors.

This problem was resolved by smoothing the experimental data. A custom data smoothing function was created to obtain a smooth, continuous experimental temperature rise. The data smoothing function consisted of the following steps:

1. The number of points (n) for which the temperature was identical were counted. The number ranged from 6 to 9.
2. If n was odd, the $(n+1)/2$ point was selected as representative of the set. If n was even, the point between $n/2$ and $(n+1)/2$ was selected as the representative at that temperature.
3. The points at each temperature were connected to get a smoothed temperature profile.

Figure 1.6 compares the uncalibrated, calibrated and smoothed data for the initial 1 s of the experiment.

While the experimental data was recorded for 200 s, the initial time interval (0 - 1 s) was found to be the most critical to understand heater response. The time t = 0 was synchronized for all experiments. The t = 0 point was selected as the time point when a sharp temperature rise was detected. Any redundant data points before the temperature rise were eliminated. Starting from the synchronized t = 0, the next 1 s was evaluated. Thus, the estimation analysis was carried out for 1 s for all experiments.

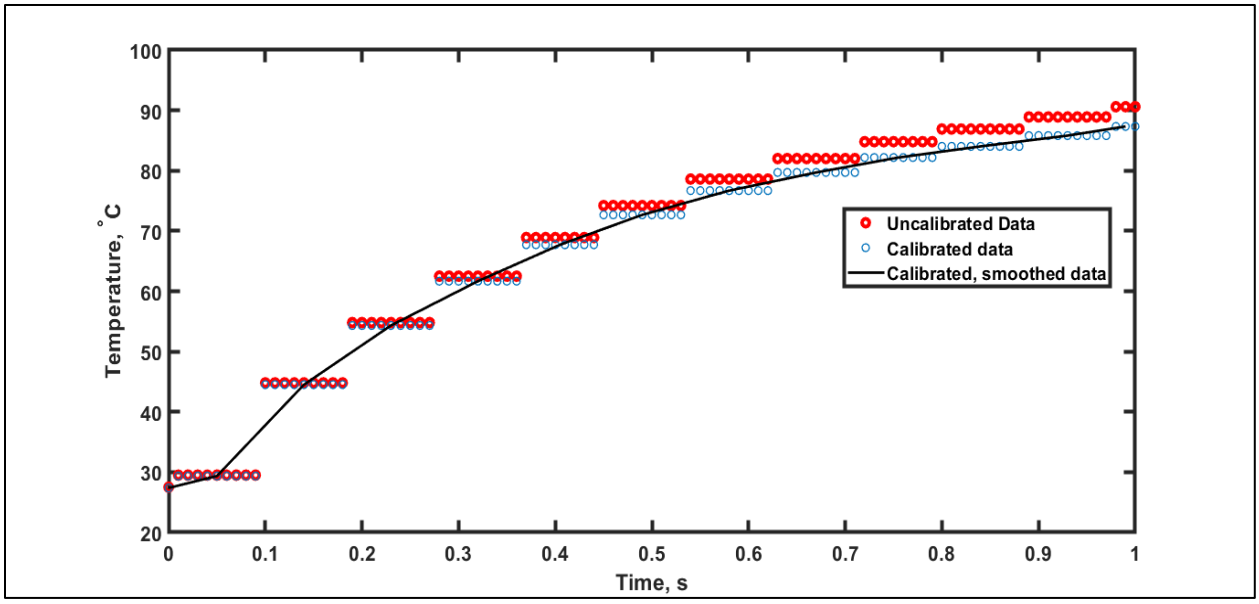

Figure 1.6 Comparison of uncalibrated, calibrated and smoothed RTD data for the first 1 s of experiment

1.4.3 Scaled Sensitivity Coefficients

Scaled sensitivity coefficients (SSCs) for k_h and C_h were calculated before the sequential estimation procedure. SSCs should be large and uncorrelated to simultaneously estimate multiple parameters (Mishra et, al, 2016). The sum of SSCs of all parameters should add up to a non-zero value to simultaneously estimate more than one parameter. In this case, the SSCs of k_h and C_h were found to be correlated, and the sum of SSCs was zero (Fig. 1.7). This indicates that from the given data, k_h and C_h cannot be independently estimated. However, the ratio of k_h and C_h, i.e. the thermal diffusivity of the material can be estimated.

$$\text{Thermal Diffusivity, } \alpha_h = \frac{k_h}{C_h}, \frac{m^2}{s} \quad \textbf{(13)}$$

Fig. 1.8 charts the SSC before the thermal diffusivity is estimated. The SSC increases initially and has a high value of 18°C at its maximum.

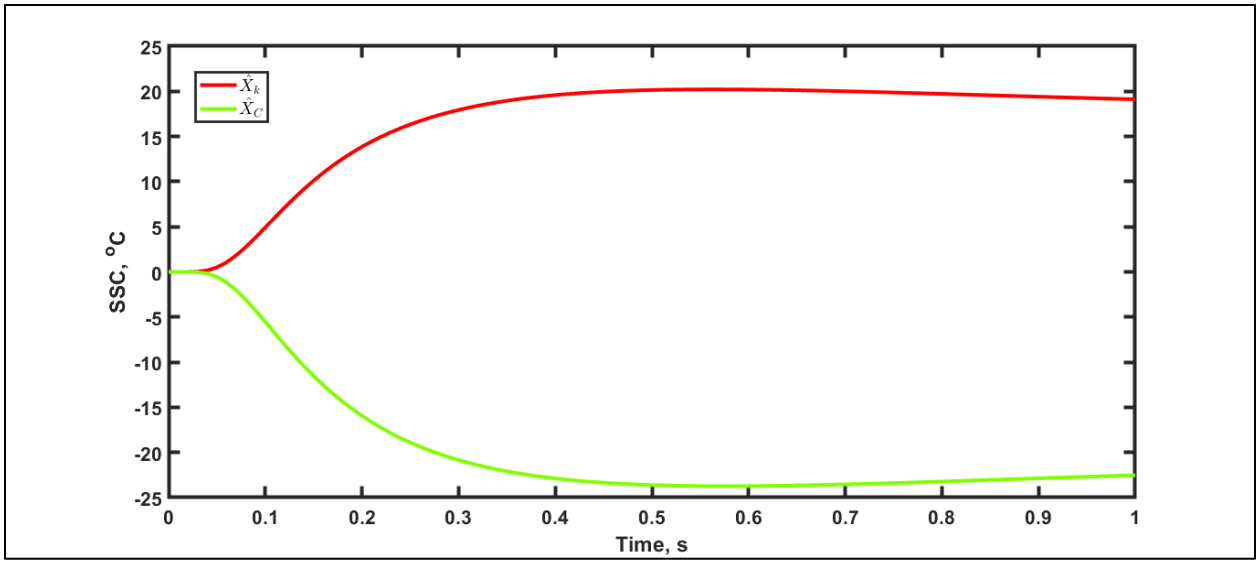

Figure 1.7 SSC for k and C for first 1 s of experiment

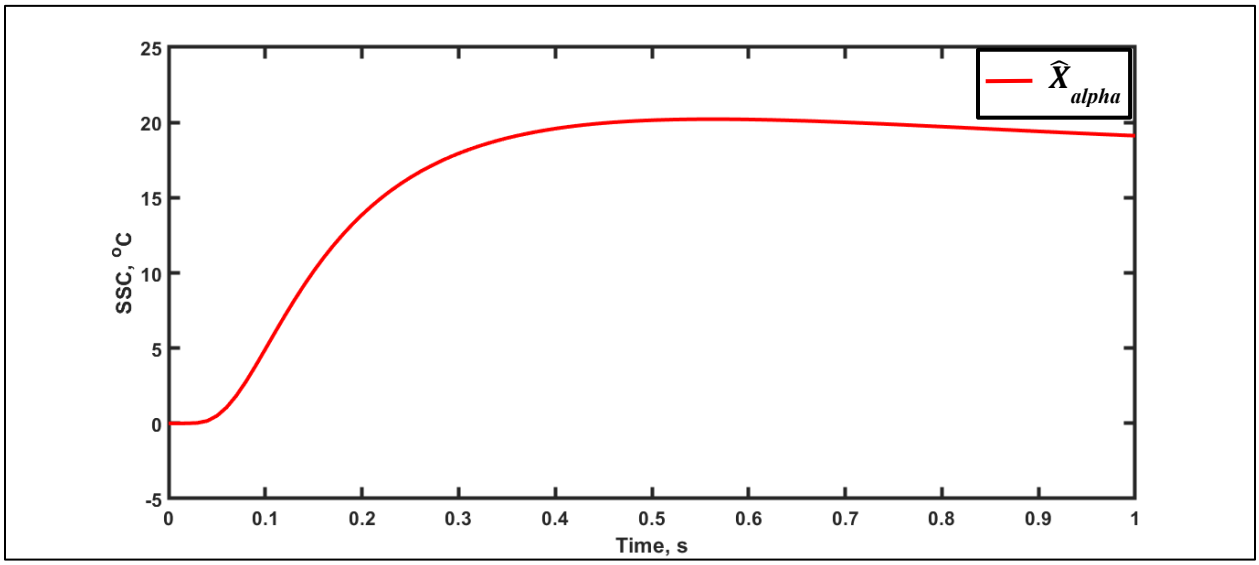

Figure 1.8 SSC for thermal diffusivity before parameter estimation for oil bath at 125°C for first 1 s

1.4.4 Sequential Estimation

Thermal diffusivity of the heater was estimated as per the procedure described in the previous section. Fig. 1.9 shows the estimated value over time. The estimated value became constant as

time progressed. The constant value indicates that the final estimated value of the parameter had been achieved and further iterations were not needed.

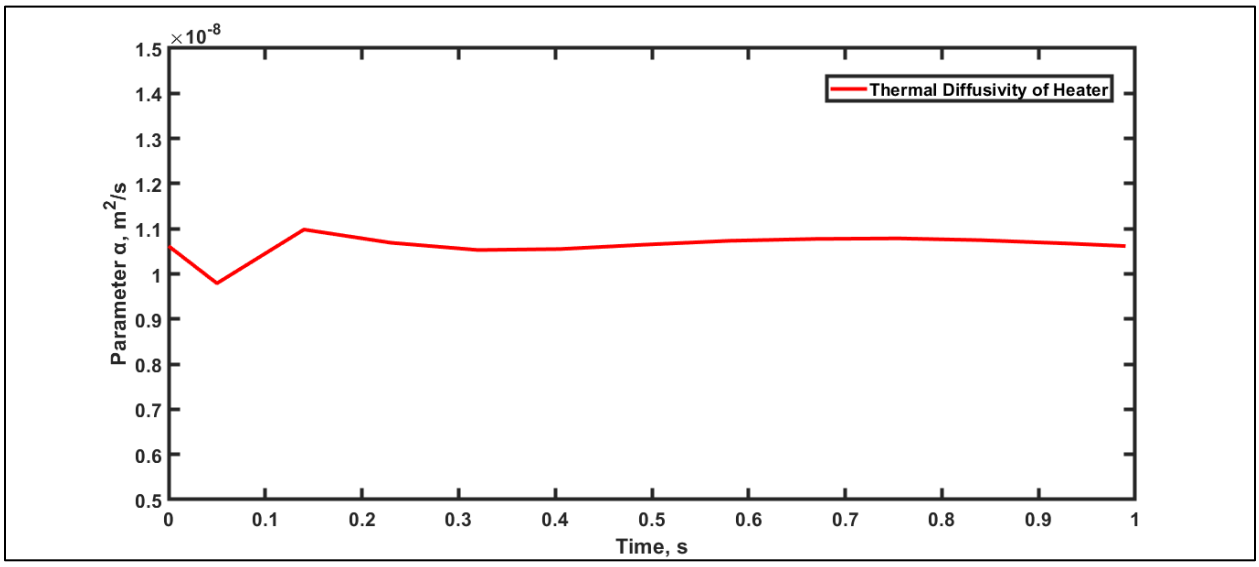

Figure 1.9 Estimated parameter value as a function of time

As a part of the estimation procedure, the sum of squares of the difference between the predicted temperature and experimental temperature was minimized at each time point. The predicted and experimental temperature at the end of the estimation procedure is shown in Fig. 1.10.

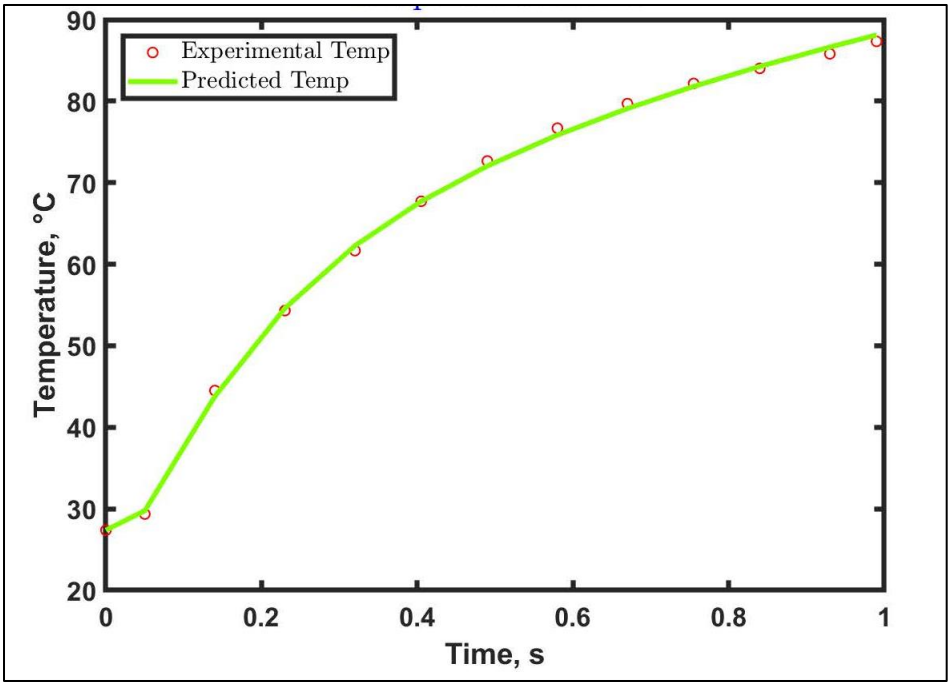

Figure 1.10 Experimental and Predicted Temperature of Heater RTD at end of estimation procedure

The difference between the experimental and predicted temperatures, called residuals, was also plotted as a function of time (Fig. 1.11). The residuals fulfill the standard statistical assumptions: additive, uncorrelated, zero mean, constant variance and normally distributed errors. The residuals are distributed around zero mean.

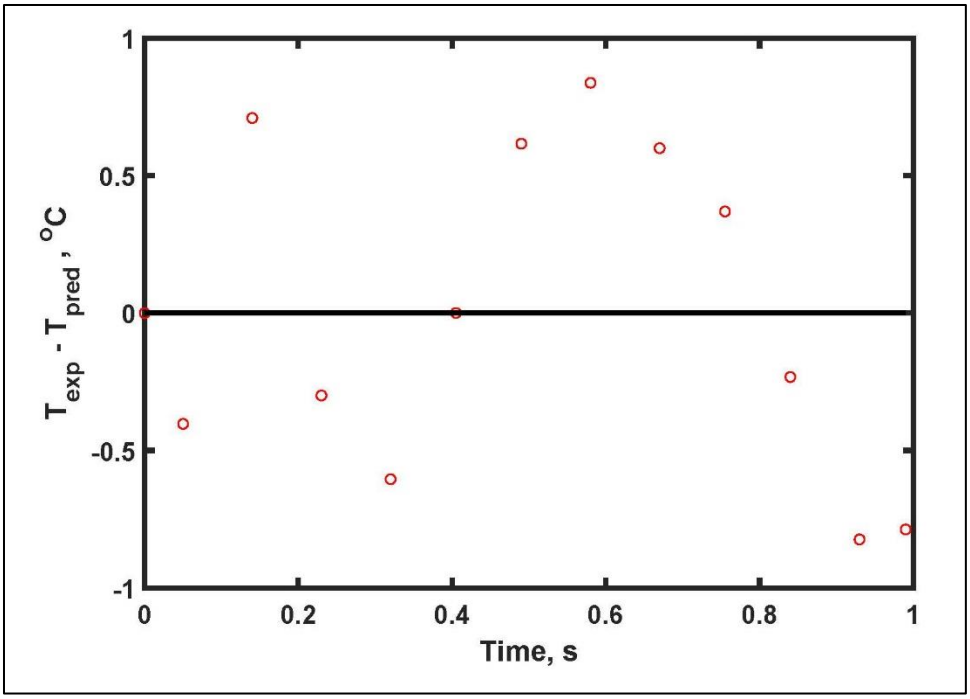

Figure 1.11 Residuals

The estimated values of thermal diffusivity at each temperature are listed in Table 1.3, 1.4 and 1.5 below:

Table 1.3 Effective thermal diffusivity of thin film heater at oil temperature 105°C

α, m^2/s	95% Confidence Interval (lower-bound)	95% Confidence Interval (upper-bound)	Standard Deviation	Root Mean Square Error
5.02×10^{-9}	4.66×10^{-9}	5.37×10^{-9}	4.16×10^{-11}	6.58×10^{-7}
4.14×10^{-9}	3.96×10^{-9}	4.29×10^{-9}	4.16×10^{-11}	3.75×10^{-7}
4.38×10^{-9}	3.92×10^{-9}	4.83×10^{-9}	4.16×10^{-11}	9.79×10^{-7}

Table 1.4 Effective thermal diffusivity of thin film heater at oil temperature 115°C

α, m^2/s	95% Confidence Interval (lower-bound)	95% Confidence Interval (upper-bound)	Standard Deviation	Root Mean Square Error
9.97×10^{-9}	9.62×10^{-9}	1.03×10^{-8}	8.33×10^{-11}	3.12×10^{-7}
1.04×10^{-8}	9.98×10^{-9}	1.09×10^{-8}	8.33×10^{-11}	3.58×10^{-7}
1.08×10^{-8}	1.00×10^{-8}	1.12×10^{-8}	8.33×10^{-11}	4.16×10^{-7}

Table 1.5 Effective thermal diffusivity of thin film heater at oil temperature 125°C

α, m^2/s	95% Confidence Interval (lower-bound)	95% Confidence Interval (upper-bound)	Standard Deviation	Root Mean Square Error
1.04×10^{-8}	1.00×10^{-8}	1.08×10^{-8}	8.33×10^{-11}	3.50×10^{-7}
1.085×10^{-8}	1.05×10^{-8}	1.12×10^{-8}	8.33×10^{-11}	2.33×10^{-7}
9.08×10^{-9}	9.17×10^{-9}	1.01×10^{-8}	8.33×10^{-11}	3.25×10^{-7}

At constant temperature and pressure, thermal diffusivity represents the tendency of a material to conduct heat relative to its tendency to store heat. Thermal diffusivity of the heater gives us detailed insight into the heat transfer pattern inside the heater. The values of thermal diffusivity can also help us determine the amount of time the heater would take to reach certain temperatures. Thermal conductivity of the heater, about 0.01- 0.02 W/mK, is very close to thermal conductivity of insulating materials (Jannot, 2008). The volumetric heat capacity (2.4×10^6 J/m^3K) is similar to the value (2.3×10^6 J/m^3K) reported by Dowding et al (1999).

The thermal diffusivity reported in Table 1.3, 1.4, 1.5 is the effective thermal diffusivity of the thin film heater. As shown in Fig. 1.1, the heater consists of layers of polyimide, Monel alloy, and Nickel 201 stuck together by bond ply. The contact resistances between these layers are not considered in the heat transfer model. While the thicknesses of the layers are theoretically known,

it was not possible to verify the same. To eliminate discrepancy around layer thickness and contact resistance, the heater was modeled as a lumped body with effective properties.

The convective heat flux provided by the oil bath is an important factor that affects the estimation of heater properties. In an oil bath, oil is heated and stirred using a propeller and motor to reach uniform temperature throughout the bath tank. Thus, the system has forced convection of oil. The convective heat transfer coefficient in an oil bath would vary based on geometry, flow conditions and type of oil used. Incorrect value of convective heat transfer coefficient of oil can lead to inaccurate values of heater properties. The value used for estimation was based on literature value used for forced convection of silicone oil. The results were consistent and precise for h = 1800 W/m^2K, used for the study.

The accuracy of parameter estimates is dependent on the accuracy of predicted and experimental data. From a modeling perspective, the model should represent reality as much as possible. If the input conditions to the simulation, for instance, geometry and physics, are the same as the experimental setup, the output data will have reduced errors. From an experimental perspective, this reduction can be achieved by minimizing errors in data acquisition, measurement and calibration of temperature-sensing elements. The heater RTD was found to have non-linear calibration. It was essential to understand the calibration trend of the temperature sensor to reduce experimental error. The residuals for this study improved significantly after the 10°C step corrections were applied. Further studies are needed to improve knowledge about the relationship of RTD temperature that is embedded inside the thin film heater with the actual temperature.

As can be observed from the results, the thermal properties of the heater change with temperature. Temperature dependency of the heater properties would be important to know while determining potential applications of the heater. The change in thermal properties with temperature can change the way a material is heated by the heater. More work is needed to quantify heater thermal properties as a function of temperature. The goal of this work was to provide information about the thin film heater that can be used to enable optimal applications.

1.5 Conclusions

The effective thermal diffusivity of a thin film heater was estimated using sequential parameter estimation. Sensitivity analysis was used to determine estimable parameters. The effective thermal diffusivity was found to be 4.51 x 10^{-9} m^2/s, 1.03 x $10^{-8}$$m^2/s$, 1.04 x 10^{-8} m^2/s at oil temperatures 105°C, 115°C, and 125°C respectively. The thermal properties of the heater were found to be temperature dependent. Additional studies are needed to thermally characterize performance of the heater for longer duration.

1.6 References

Ahadi, M., Andisheh-Tadbir, M., Tam, M., & Bahrami, M. (2016). An improved transient plane source method for measuring thermal conductivity of thin films: Deconvoluting thermal contact resistance. *International Journal of Heat and Mass Transfer*, *96*, 371–380. https://doi.org/10.1016/j.ijheatmasstransfer.2016.01.037

AutomationDirect.com, Cumming, Georgia

Beckhoff Automation GmbH & Co. KG, Verl, Germany

Beck, J.V., Arnold, K.J., (1977) Parameter Estimation in Engineering and Science. Wiley

COMSOL Inc., Burlington, MA

E. Sweat, V., & G. Haugh, C. (1974). A Thermal Conductivity Probe for Small Food Samples. *Transactions of the ASAE*, *17*(1), 56–0058. https://doi.org/10.13031/2013.36786

Golan, G., Axelevitch, A., Sigalov, B., & Gorenstein, B. (2003). Integrated thin film heater-thermocouple systems. *Microelectronics Reliability*, *43*(3), 509–512. https://doi.org/10.1016/S0026-2714(02)00320-7

Greiby, I., Mishra, D. K., & Dolan, K. D. (2014). Inverse method to sequentially estimate temperature-dependent thermal conductivity of cherry pomace during nonisothermal heating. *Journal of Food Engineering*, *127*, 16–23. https://doi.org/10.1016/j.jfoodeng.2013.10.039

Gustafsson, S. E. (1991). Transient plane source techniques for thermal conductivity and thermal diffusivity measurements of solid materials. *Review of Scientific Instruments*, *62*(3), 797–804. https://doi.org/10.1063/1.1142087

Herzen, R. V., & Maxwell, A. E. (1959). The measurement of thermal conductivity of deep-sea sediments by a needle-probe method. *Journal of Geophysical Research (1896-1977)*, *64*(10), 1557–1563. https://doi.org/10.1029/JZ064i010p01557

Huang, C.-H., & Huang, C.-Y. (2007). An inverse problem in estimating simultaneously the effective thermal conductivity and volumetric heat capacity of biological tissue. *Applied Mathematical Modelling*, *31*(9), 1785–1797. https://doi.org/10.1016/j.apm.2006.06.002

Huang, L., & Liu, L.-S. (2009). Simultaneous determination of thermal conductivity and thermal diffusivity of food and agricultural materials using a transient plane-source method. *Journal of Food Engineering*, *95*(1), 179–185. https://doi.org/10.1016/j.jfoodeng.2009.04.024

Incropera, F. P., Lavine, A. S., Bergman, T. L., & DeWitt, D. P. (2007). *Fundamentals of heat and mass transfer*. Wiley.

Jannot, Y., Degiovanni, A., & Payet, G. (2009). Thermal conductivity measurement of insulating materials with a three layers device. *International Journal of Heat and Mass Transfer*, *52*(5), 1105–1111. https://doi.org/10.1016/j.ijheatmasstransfer.2008.09.017

Kevin J. Dowding, R. J. C., Bennie F. Blackwell. (1999). Application of Sensitivity Coefficients for Heat Conduction Problems. *Numerical Heat Transfer, Part B: Fundamentals*, *36*(1), 33–55. https://doi.org/10.1080/104077999275767

Mishra, D. K., Dolan, K. D., Beck, J. V., & Ozadali, F. (2016). A novel instrument for rapid measurement of temperature-dependent thermal properties of conduction-heated food up to 140 °C. *Journal of Food Engineering*, *191*, 19–27. https://doi.org/10.1016/j.jfoodeng.2016.06.028

Neitzert, H. C., Vertuccio, L., & Sorrentino, A. (2011). Epoxy/MWCNT Composite as Temperature Sensor and Electrical Heating Element. *IEEE Transactions on Nanotechnology*, *10*(4), 688–693. https://doi.org/10.1109/TNANO.2010.2068307

Saad, A., Echchelh, A., Hattabi, M., & El Ganaoui, M. (2014). The identification of effective thermal conductivity for fibrous reinforcement composite by inverse method. *Journal of Reinforced Plastics and Composites*, *33*(23), 2183–2191. https://doi.org/10.1177/0731684414556011

Telejko, T. (2004). Analysis of an inverse method of simultaneous determination of thermal conductivity and heat of phase transformation in steels. *Journal of Materials Processing Technology*, *155–156*, 1317–1323. https://doi.org/10.1016/j.jmatprotec.2004.04.185

Zohuri, B., & Fathi, N. (2015). Forced Convection Heat Transfer. In B. Zohuri & N. Fathi (Eds.), *Thermal-Hydraulic Analysis of Nuclear Reactors* (pp. 267–285). Springer International Publishing. https://doi.org/10.1007/978-3-319-17434-1_9

CHAPTER 2. DESIGN AND OPTIMIZATION OF COMPLEMENTARY EXPERIMENTS FOR MULTIPLE PARAMETER ESTIMATION IN HEAT TRANSFER MODEL

2.1 Abstract

Thermal properties of food are critical for designing efficient thermal processes for food manufacturing. Current methods to measure temperature-dependent thermal properties of foods are costly, time consuming and labor intensive, with certain methods requiring composition analysis. A novel method of complementary experiments was used in this study for simultaneous estimation of temperature-dependent thermal conductivity (k) and specific heat capacity (C).

The design of complementary experiments was done in two parts. In the first part, the designs were simulated and compared. Three types of heating profiles were evaluated. The first heating profile used only one heat source and one temperature measurement. The subsequent two profiles were complementary experiments in which two heaters and two temperature measurements were used. The concentrically arranged heaters each had an embedded resistance temperature detector (RTD). For each profile, the sensitivity coefficients for both k and C at temperatures T_1 and T_2 respectively, were calculated. Maximization of the determinant of the sensitivity matrix was defined as the optimality criterion (Δ). For each simulated profile, the scaled sensitivity coefficients of the four parameters (k_1, k_2, C_1, C_2) and Δ were compared. The number of parameters that could be estimated was determined using sensitivity analysis.

The simulated results were verified experimentally using Thermal Properties Cell (TPCell), a custom made bench scale device. Sequential parameter estimation was used to estimate the thermal properties of sweet potato puree. The thermal conductivity and specific heat capacity of sweet potato puree at 25°C were found to be 0.532 W/mK and 3.562 x 10^6 J/kgK respectively. The estimated values closely matched values from published literature.

2.2 Introduction

Thermal processing of foods has revolutionized the food industry since its inception in the early 19th century (Featherstone, 2011). Heat processing is one of the most commonly used methods to ensure the safety and quality of food products. To design an efficient thermal process, it is essential to know the thermal properties of the food products. Thermal properties, namely thermal conductivity (k), volumetric heat capacity (C) and thermal diffusivity (α), govern the thermal response of the food matrix. The properties are dependent on factors such as temperature and composition of the food products (Choi, 1985). Existing methods for measurement of food thermal properties are divided broadly into two categories: steady state and transient state.

Steady state methods rely on temperature equilibrium in the sample. In other words, the entire sample volume must be heated to the specified temperature for accurate measurement. Steady state methods are time consuming, taking up to 12 hours (Murakami & Okos, 1989). Moreover, food samples undergo significant changes in texture and composition with temperature. The thermal properties measured when the sample reaches thermal equilibrium may not be an accurate representation of the original sample.

Transient methods measure thermal properties in a transient, non-isothermal state. Line source and plane source are two of the commonly used transient methods. The transient line source method typically consists of a small probe inserted in a small food sample. A thermocouple and a hot-wire are placed in the probe (Sweat and Haugh, 1974). The heating of the hot-wire creates a change in the temperature of the food material in the surrounding. This increase in temperature, measured by the thermocouple, is used to calculate the thermal conductivity of the sample.

Gustafsson developed the idea of transient plane source method (1991). A temperature sensor, usually disk or square shaped, is placed between two identical samples. The temperature sensor is used as a heat source as well as temperature indicator (Huang and Liu, 2009, Ahadi et. al, 2016). The sensor is heated by providing electrical current. The increase in temperature causes a temperature change on samples placed on either side. This increase is correlated with the thermal properties of sample.

Commercial devices based on both methods are available. KD2 Pro, a commercial device by Decagon, Inc. is based on transient line source theory, with the ability to attach various sensor probes based on state (solid or liquid), viscosity, and moisture content of materials. One of the major shortcomings with this device is that the temperature sensor must be equilibrated to the sample temperature, considerably extending the experimental time. It was also found that with repeated use, sensors failed at high temperatures (above 100°C) and thermal conductivity could not be measured (Mishra et al., 2016).

Mathematical modeling has been used extensively to estimate food thermal properties. Predictive models were developed by Choi and Okos incorporating the effect of temperature and composition on thermal conductivity (1986). Mathematical modeling, coupled with inverse techniques is a powerful tool to estimate the thermophysical properties of a wide variety of foods.

An inverse method was used by Monteau et. al to estimate the thermal conductivity of sandwich bread during cooling (2008). A polynomial expression was derived for thermal conductivity as a function of temperature and local water content. In another study, the thermal properties of frozen green beans obtained by conventional experimental methods were compared to those obtained by inverse methods (Martins and Silva, 2004). The inverse problem methodolody was applied to determine the apparent thermal conductivity of carrot puree during freezing by Mariani et. al (2009).

In food thermal properties literature, various inverse methods have been utilized depending on the food product, geometry, experimental data and availability of mathematical models. In recent years, there has been an increased focus on sequential parameter estimation. Sequential estimation is based on the matrix inversion lemma and Gauss-minimization method. The values of the parameters are updated iteratively. The sequential estimation procedure provides more insight into the estimation process and traces the variation of the estimates with respect to the response data and time. The trend of estimation can help with the design of experiments (Beck and Woodbury, 1998).

A FORTRAN code was developed by Mohammad (2009) based on sequential parameter estimation to simultaneously estimate volumetric heat capacity and thermal conductivity of conduction-heated foods. The computer program was validated using simulated temperature data. In a follow-up work, an experimental apparatus was developed to record transient temperature measurements and estimate the thermal diffusivity of lean beef (Mohammad, 2010). The sequential estimation method was used by Greiby et. al (2014) to determine the temperature-dependent thermal conductivity of cherry pomace during non-isothermal heating. The technique was also applied by Muramatsu et. al (2017) for measuring thermal diffusivity of low-moisture foods including almond meal, cornmeal, wheat flour, and peanut butter.

Inverse methods rely on estimating parameters (k, C, α) from experimental data (Temperature). The feasibility of determining one or more parameters from a given set of experimental data depends on sensitivity coefficients of each parameter. Hence, the maximum information that can be obtained from a single experiment depends on the sensitivity coefficients. Sensitivity coefficients indicate the extent of change in a measured variable due to a change in the value of an input parameter. Sensitivity coefficients should be large and uncorrelated to accurately and simultaneously estimate multiple parameters.

Based on sensitivity analysis, a series of experiments known as complementary experiments, can be designed and optimized. Complementary experiments can be conducted on the same experimental setup in a single overall experiment, by varying heat transfer profiles and/or geometry. Complementary experiments were defined as “a set of experiments in which each experiment provides information that is not correlated in the same way as the previous one” (McMasters et al. (2017). For instance, in the complementary experiments proposed in the paper, the first experiment could estimate only the product of k and C. The second experiment, complementary to the first one, could estimate only the ratio of k and C. In both experiments, the thermal parameters were correlated, but in different ways. When conducted as individual experiments, neither of the two experiments could simultaneously estimate k and C. However, if the two experiments were combined and conducted as a single complementary experiment, both k and C could be estimated at the same time from the same data. In the work of McMasters et. al,

the geometric configurations were changed to generate complementary experiments for multi-parameter estimation.

In the current work, heating profiles are changed to conduct complementary experiments. The advantages of complementary experiments are that the experimental set-up does not need be changed. Secondly, unlike other experiments, multiple parameters can be estimated from the same temperature-time profile.

Optimal Experimental Design:

Finding optimal experiments is one of the fundamental types of parameter estimation problems (Beck and Arnold, 1977). The criterion used to distinguish an optimal experiment from a given set of experiments is based on the minimization of hyper-volume of the confidence region. The criterion is derived based on the following standard assumptions in the measurement error: additive, zero mean, constant variance, independent, normally distributed errors.

To estimate two or more parameters, an optimal experiment should have the largest value of the determinant of the sensitivity matrix. Mathematically,

$$\Delta = \max \left| X^T X \right| \tag{14}$$

For n measurements, conducted to estimate p parameters, the criterion becomes:

$$\max \Delta^n = \max \frac{\Delta}{n^p} \tag{15}$$

For two parameters (p = 2), with n measurements, the equation reduces to

$$\Delta^n = \frac{\Delta}{n^2} \tag{16}$$

Assuming the measurements are uniformly spaced in time, from t = 0 to t = t_n, for p = 2,

$$\Delta^n = C_{11}C_{22} - C_{12}^2 \tag{17}$$

$$\text{where } C_{ij} = \frac{1}{t^n}\int_0^{t_n} X_i(t)\, X_j(t) dt \tag{18}$$

where $X_i(t)$ is the sensitivity coefficient for each parameter i and time t. The same approach is applied when p = 4.

2.2.1 Objective

The objective of this study is to determine the optimal design of complementary experiments for the simultaneous estimation of temperature-dependent thermal conductivity and volumetric heat capacity.

2.3 Materials and Methods

2.3.1 Experimental Setup

A unique benchtop tool, called "Thermal Properties Cell (TPCell)" was custom-made to run complementary experiments. The main assembly comprised of several parts: two thin film heaters, a stainless steel (SS) base, SS sample holder, and a pressure cap.

The thin film heaters referred to as "Inner Heater" and "Outer Heater" respectively, were selected for their rapid temperature response. The thin film heaters were hollow cylinders, each with a thickness of 0.015". The inner heater, 0.25" OD x 6" in dimensions, was mounted on a hollow stainless-steel cylinder. The outer heater 0.75" ID x 6" in dimensions was supported by a SS sleeve on the outer side. Both thin film heaters had a Monel heat source sandwiched within layers of polyimide. A Nickel 201 RTD was embedded in the central area of the hollow cylinders. An aluminum backing was added to the heaters to increase mechanical rigidity. The bond-ply was used to stick the layers together.

The SS base was used to retain the inner and outer heaters and the supporting SS cylinders. The SS sample holder was custom made to fit between the inner and outer heaters. The sample holder had an inner and outer tube that matched the shape of the inner and outer heater. The sample held within the holder took the shape of an annulus. The top of the sample holder had a flange to mate with the pressure cap and created a pressure seal for the experiment as shown in Fig. 2.1.

The prototype was pressurized to prevent boiling and inhibit moisture migration during the experiment. For this purpose, the SS pressure cap was designed to seal the prototype. A seal made of high-durometer silicone, which mated with the SS sample holder, was used. The pressure cap was equipped with a check valve integrated into the inlet to prevent the material from feeding back into the supply line. It also had a pressure

relief valve with a filter to relieve the system pressure after the experiment was finished. The sample chamber was pressurized using compressed air.

A cooling jacket made of copper coils was wrapped around the outer sleeve. The jacket was used to provide uniform conditions during the experiment and reduce the impact of ambient conditions. The cooling jacket also reduced the time taken by the heaters to return to room temperature after the experiment was done. A small pump and reservoir were added to recirculate the coolant (water) in the cooling jacket.

A control and data acquisition system was built using PC-based hardware from Beckhoff Automation. Heater power control and measurement were done using a Beckhoff EL7342. RTD measurements were performed using a Beckhoff EL3202. Control and measurement were done using custom PLC software with control and data acquisition at a rate of 100 Hz. Additionally, a custom PC UI software was developed to interface with the PLC and save test data.

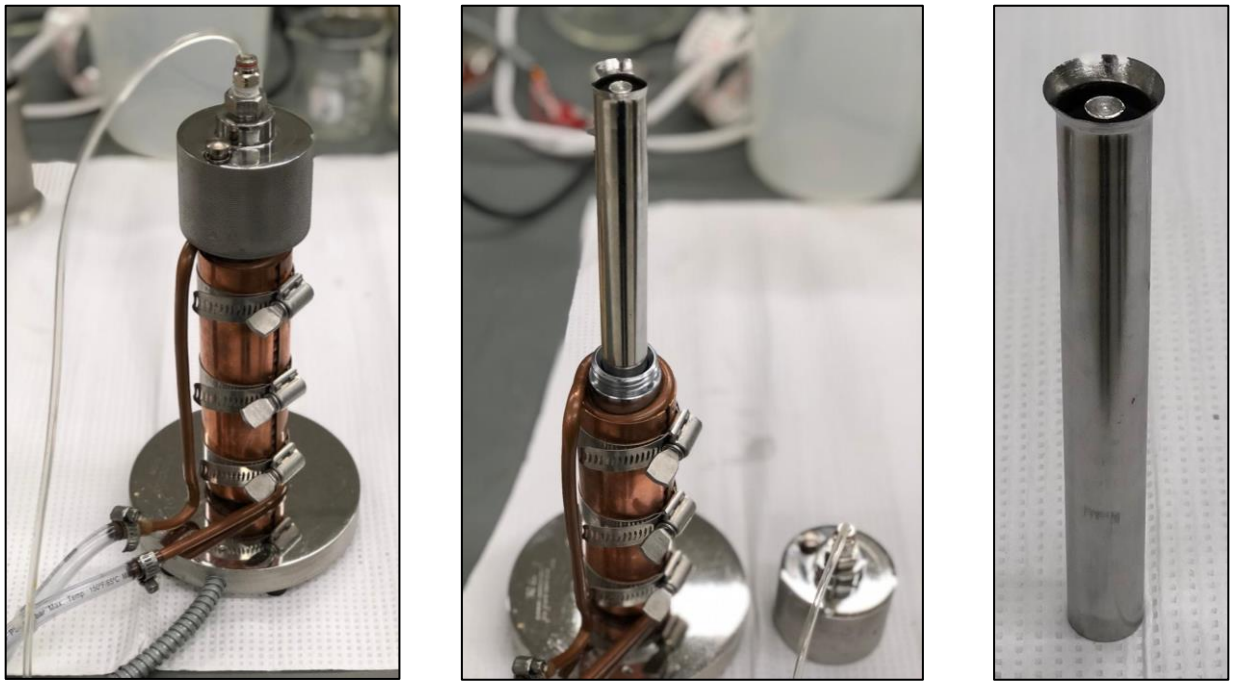

Figure 2.1: (a) TPCell Assembly (b) Sample holder being inserted (c) Sample holder with mating flange

2.3.2 Mathematical Model

The TPCell design is based on transient heat conduction in a cylinder. Fig. 2.2 shows the schematic 1D diagram of the arrangement.

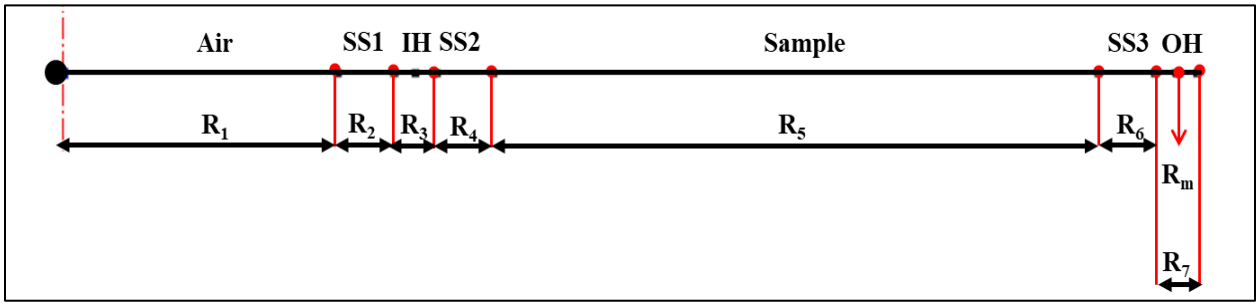

Figure 2.2 1D schematic of TPCell

Air – Air inside the hollow steel cylinder on which the inner heater is wrapped

SS1 – Thickness of the hollow stainless-steel cylinder

IH – Inner heater

SS2 – Thickness of inner layer of stainless-steel sample tube

Sample – Annular space to fill sample in the sample tube

SS3 – Thickness of outer layer of stainless-steel sample tube

OH – Outer heater

The system is described by the following set of equations (Eq. 19-22):

$$\frac{1}{r}\frac{\partial}{\partial r}\left[k_a r\frac{\partial T}{\partial r}\right]=C_a\frac{\partial T}{\partial t}\ \text{for}\ 0<r\le R_1, t>0 \qquad \textbf{(19)}$$

$$\frac{1}{r}\frac{\partial}{\partial r}\left[k_s r\frac{\partial T}{\partial r}\right]=C_s\frac{\partial T}{\partial t}\ \text{for}\ R_1<r\le R_2, R_3<r\le R_4, R_5<r\le R_6, t>0 \qquad \textbf{(20)}$$

$$\frac{1}{r}\frac{\partial}{\partial r}\left[k_h r\frac{\partial T}{\partial r}\right]+g_0 f\left(t\right)=C_h\frac{\partial T}{\partial t}\ \text{for}\ R_2<r\le R_3, t>0 \qquad \textbf{(21)}$$

$$\frac{1}{r}\frac{\partial}{\partial r}\left[k(T)\,r\,\frac{\partial T}{\partial r}\right]=C(T)\frac{\partial T}{\partial t}\ \text{ for } R_4<r\le R_5, t>0 \tag{22}$$

The initial temperature is:

$$T(r,0)=T_0 \tag{23}$$

The boundary condition at R_m is:

$$T(R_m,t)=(T_0)\,f_1(t)\ \text{ where } R_m \text{ is the midpoint between } R_6 \text{ and } R_7 \tag{24}$$

A linear relationship with temperature is assumed for thermal conductivity and volumetric heat capacity, as described by Eq. 25-26.

$$k(T)=k_1\left(\frac{T_2-T}{T_2-T_1}\right)+k_2\left(\frac{T-T_1}{T_2-T_1}\right) \tag{25}$$

$$C(T)=C_1\left(\frac{T_2-T}{T_2-T_1}\right)+C_2\left(\frac{T-T_1}{T_2-T_1}\right) \tag{26}$$

where T_1 and T_2 are reference temperatures.

The 1D model was solved using finite element method in COMSOL Multiphysics.

2.3.3 Designs of Experiment

The experiment was divided into two approaches. The first approach used simulations. Learnings from the first approach were utilized to gather experimental data using TPCell.

The COMSOL model was a simulated replica of TPCell. The geometry and thermal properties of the components such as SS sample holder, thin film heaters, etc. were added to the TPCell COMSOL model. The thin film heater properties estimated in Chapter 1 were used for the inner heater.

Properties of sweet potato puree were used as sample properties in the simulation and it was also used for experimental runs. It can be assumed that due to its high viscosity, the semi liquid sweet potato puree has negligible convective currents within the sample. The semi-liquid nature also promotes better contact between sample and walls of the sample holder, thereby reducing contact resistance.

In both, simulations and experiments, the power provided to the respective heaters resulted in increased temperatures measured by respective RTDs. The COMSOL model provided flexibility to try various combinations of power profiles for the inner and outer heater without the loss of experimental resources. It was quicker to check the impact on sensitivity analysis and Δ using simulations. Sensitivity analysis provided insight into expected results. It was used to predict parameters that could potentially be estimated from each data set.

Simulated Power and Temperature Profiles

1. *Step Pulse of Power Provided Only to Inner Heater*

In this profile, the system was initially at room temperature. 38 W of power was instantaneously provided to the inner heater for 30 s. As a result, the temperature of the inner RTD increased to 138℃ from ambient temperature (25℃). The magnitude of power was decided based on the required temperature rise. The experiment ended once the inner RTD reached the desired temperature (Fig. 2.3).

This was not a complementary experiment. The power was supplied to only one heater with the temperature being measured only at one point in the system. The following describes complementary experiments with two power profiles, one for each heater, and temperature measurements at two distinct locations.

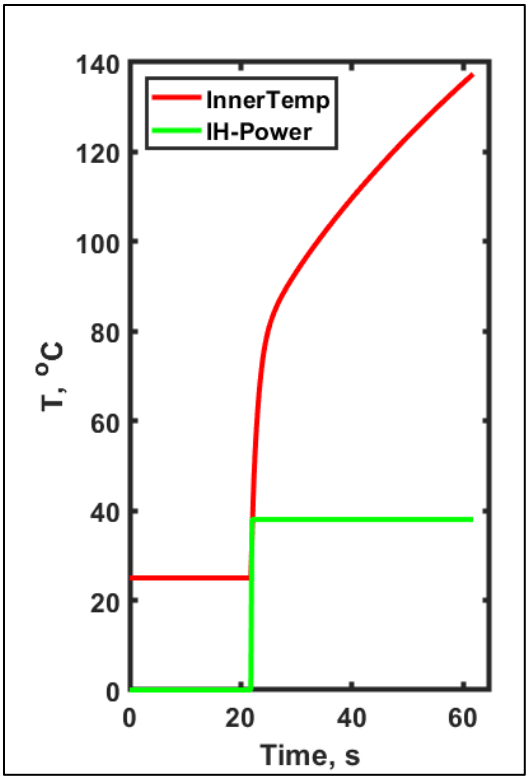

Figure 2.3 Simulated power and inner RTD profile for a step pulse of power

2. Step Pulse of Power to Inner Heater, Outer RTD Maintained at Constant Temperature

In this heating configuration, at the beginning of the experiment, no power was provided to the inner heater. Power to the outer heater was regulated in such a way that the outer RTD temperature increased from room temperature to 50°C, and remained at 50°C for the remainder of the experiment. The inner RTD temperature was continuously monitored throughout the experiment. The temperature of the inner RTD rose in response to the heat flux provided by the outer heater. As the inner RTD temperature reached a plateau close to outer RTD temperature (50°C), 21 W of power was provided to the inner heater for 120 s. This step pulse of power increased the inner RTD temperature to 138°C (Fig. 2.4).

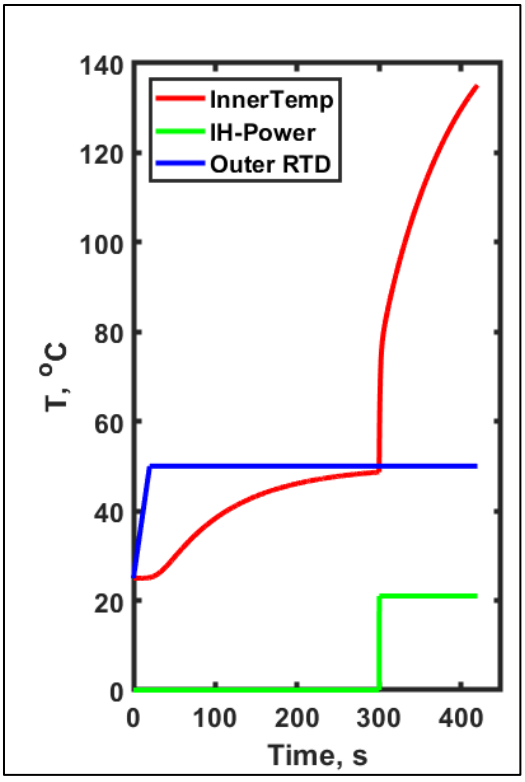

Figure 2.4 Simulated power, inner RTD and outer RTD temperature profiles for step pulse of power to inner heater and outer RTD maintained at 50°C

3. *Combination Pulse of Power to Inner Heater, Outer RTD Maintained at Constant Temperature*

In this trial, similar to the case 2, the inner heater was provided zero power in the initial part of the experiment. Meanwhile, the outer RTD temperature was increased and maintained at 50°C. In the complementary experiment, as the inner RTD approached 50°C, power was provided to the inner heater. This power profile was a combination of two functions: exponential and sinusoidal. In the first interval, the power increased exponentially from zero to 25 W. In the next interval, the power function was a decaying sinusoidal wave for 200 s. In the final interval, the inner heater power was exponentially reduced to zero in 20 s. In contrast to the other power profiles (cases 1 and 2), cooling (reduction of power) was also modeled in this heating configuration.

This combination power profile yielded an interesting temperature profile of the inner RTD. In the first interval, inner RTD temperature increased rapidly in an exponential manner. In the second

interval, the temperature increased sinusoidally, reaching 140°C by the end of the interval. In the final interval, the temperature dropped down quickly as the power decreased (Fig. 2.5).

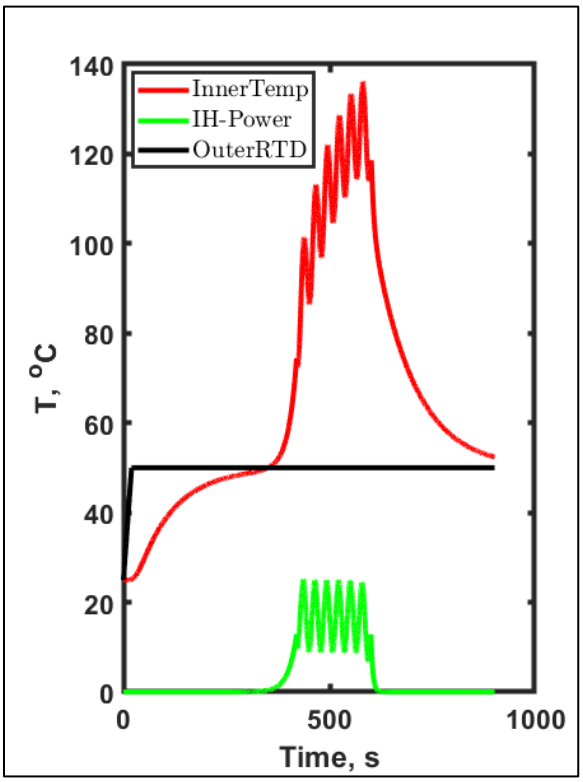

Figure 2.5 Simulated power, inner RTD and outer RTD temperature profiles for combination pulse of power to inner heater and outer RTD maintained at 50°C

For each power profile, the scaled sensitivity coefficient was calculated for four parameters at each time point: thermal conductivity of sweet potato puree at 25°C (k_1), volumetric heat capacity of sweet potato puree at 25°C (C_1), thermal conductivity of sweet potato puree at 135°C (k_2) and volumetric heat capacity of sweet potato puree at 135°C (C_2). The Δ value was also calculated as a function of time. The Δ value was normalized with the maximum power supplied.

Experimental Trials: Data Acquisition and Analysis

After analyzing the simulation results, experiments were carried out in TPCell. The intent was to conduct experimental validation for both types of complementary experiments described (cases 2 and 3). However, due to control system limitations, the sinusoidal power pulse could not be implemented experimentally.

Heater Calibration and Sample Preparation

The inner heater and outer heater were calibrated using a calibration oil bath (Fluke Calibration, 6109A portable bath). The RTD temperatures were corrected in a step-wise procedure described in Chapter 1, Section 1.2.2. Sweet potato puree was used as the sample for the experiments. 38 g of the puree was weighed and carefully poured into the sample tube while ensuring no air bubbles got trapped in the matrix. In the TPCell assembly, two solid surfaces (the heater and sample tube) were in contact. To minimize contact resistance, the two heater-sample tube interfaces (inner and outer) were greased with 4 mL of silicone lubricating grease. The grease facilitated heat flow through the assembly.

Complementary Experiment Details

Before the start of the experiment, the sample chamber was pressurized to 60 psig to prevent phase change reactions in the puree. In the initial part of the experiment, the outer heater was gradually ramped to and held at a constant temperature of 50°C. The rise in inner temperature in response to this heat flux was recorded at the inner RTD. In the complementary experiment, the inner heater was supplied with a 20 W power pulse for 140 s, while the outer RTD was maintained at 50°C. The inner temperature ramped up to temperatures in the range of 135-140°C. The inner heater was then allowed to cool, while the outer heater continued to be at 50°C. After the test was complete, both heaters were cooled to ambient temperatures. Water at room temperature was constantly circulated in the jacket throughout the experiment.

Data Analysis

The COMSOL model was used to generate predicted inner RTD temperature data for the experiment described. The SSCs were calculated for k_1, k_2, C_1, and C_2. Based on values and correlations of SSCs, the parameters were categorized as estimable and not estimable. The estimable parameters were estimated using sequential estimation.

2.4 Results and Discussion

2.4.1 Simulated Power and Temperature Profiles

The results of the first approach are discussed below. For each heating configuration, three plots are plotted as functions of time: the simulated power and inner RTD profiles, the SSCs for four parameters, and the Δ.

1. Step Pulse of Power Provided Only to Inner Heater

For this case the plots are shown in Fig. 2.6. In Fig. 2.6 (a), "InnerTemp" refers to the temperature of the inner RTD and "IH-Power" refers to power supplied to the inner heater.

The SSCs are denoted for each of the four parameters in Fig. 2.6(b). Relative to the temperature rise of more than 100°C, the sensitivities for k_2 and C_2 are extremely small (less than 1 % of the temperature rise). The sum of SSCs of k_1 and C_1 was zero. Similarly, the sum of SSCs of k_2 and C_2 was zero. This indicates that the sensitivities for k_1 and k_2 are correlated with C_1 and C_2 respectively for the entire duration of the experiment (Mishra et. al, 2017).

As seen in Fig 2.6 (c), the maximum Δ value is extremely low (order of 10^{-16}).

Thus, from this profile, the only parameter that can be estimated with maximum accuracy is α_1.

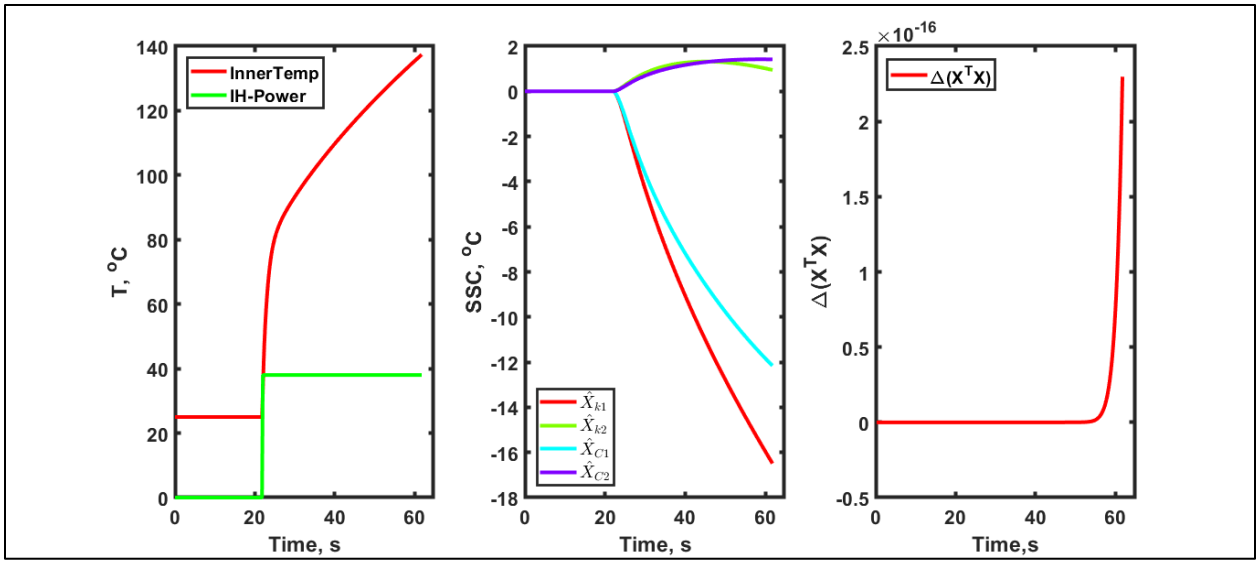

Figure 2.6 (a) Power and Temperature profile (b) SSCs for four parameters (c) Δ

2. Step Pulse of Power to Inner Heater, Outer RTD Maintained at Constant Temperature

Fig. 2.7 shows relevant graphs for step power heating profile in case 2. In Fig. 2.7(a), "Outer RTD" is the temperature of the RTD embedded in the outer heater. The significant impact of the complementary experiment can be seen from the results. The maximum Δ value for this case is 13 orders of magnitude larger than Δ for the previous case (Fig 2.7 (c)). The inclusion of the outer heater, maintained at 50°C, considerably improves the design of the experiment.

For the first part of the experiment, in which inner RTD temperature rises due to higher outer RTD temperature, SSCs for k_1 and k_2 are correlated with C_1 and C_2 respectively (Fig 2.7(b)). After 300 s, k_1 continues to have the largest SSC. However, it is important to note that the SSC for C_1 has increased and is not correlated with the SSC of k_1. It is possible to estimate both k_1 and C_1 from this case. Thus, using a complementary experiment, k_1 and C_1 can be simultaneously estimated. On the other hand, SSCs for k_2 and C_2 are quite low (less than 5% of temperature rise) making them unfit for estimation.

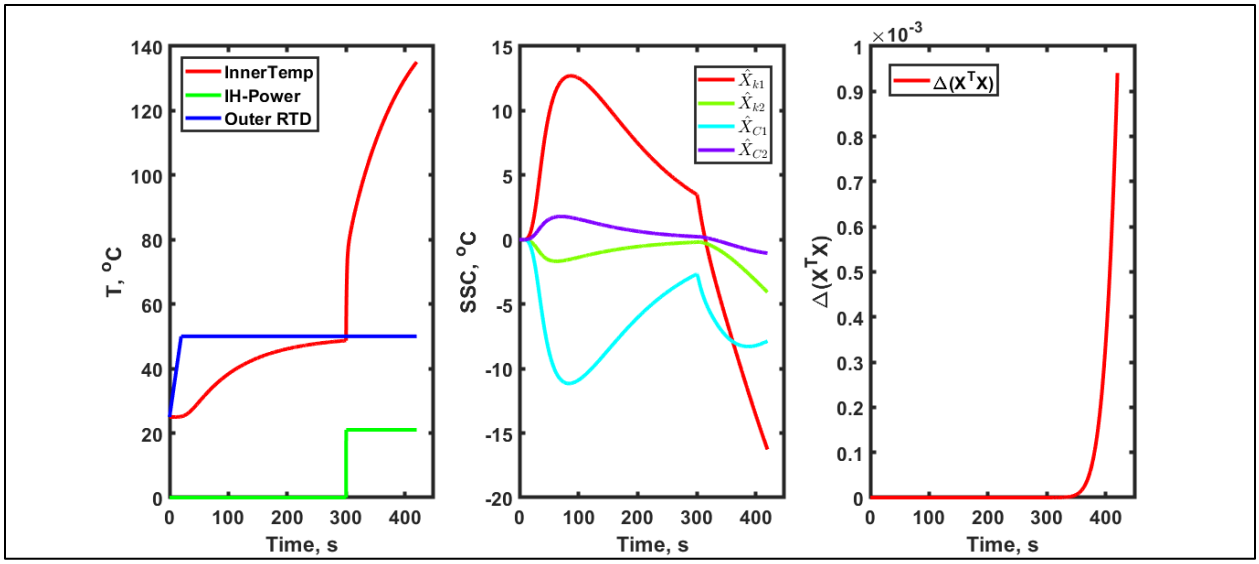

Figure 2.7 (a) Power and Temperature profile (b) SSCs for four parameters (c) Δ for a complementary experiment profile for k_h = 0.01 W/mK

One of the major factors affecting the temperature-power-time profile is thermal properties of the inner heater. Properties of the outer heater did not have a significant impact on the profile. This could be attributed to the outer RTD being maintained at a constant temperature throughout the experiment. Properties of the inner heater used for the simulations in Fig. 2.6 and Fig 2.7 are: k_h = 0.01 W/mK and C_h = 2.4x10^6 J/m^{3}K (from Chapter 1). To check the effect of heater thermal conductivity, k_h was changed to 0.2 W/mK. The result for the modified k_h for this complementary experiment is shown in Fig. 2.8.

The strong influence of k_h can be observed from the data. Compared to the maximum Δ value of 0.9 x 10^{-3} in Fig. 2.7, the maximum Δ increases to 0.07 in Fig. 2.8 (c). The amount of power required (40W) is almost double the power required in the previous case (21W) for the same temperature rise. An increase in thermal conductivity means that the heat is passed on faster to the subsequent layers and less heat is retained, resulting in lower temperature rise. To compensate for the increased rate of heat conduction, the power required is higher.

For the same temperature profile, the SSCs look starkly different (Fig. 2.8(b)). The SSC of k_2 increased considerably from Fig. 2.7(b) (from a maximum value of 4°C to 22°C). Thus, in addition to k_1 and C_1, k_2 can also be estimated from this heating profile. By changing k_h, the complementary

experiment improved, making it possible to simultaneously estimate three parameters from a single experiment. Thus, a heater with better thermal conductivity results in a better experiment.

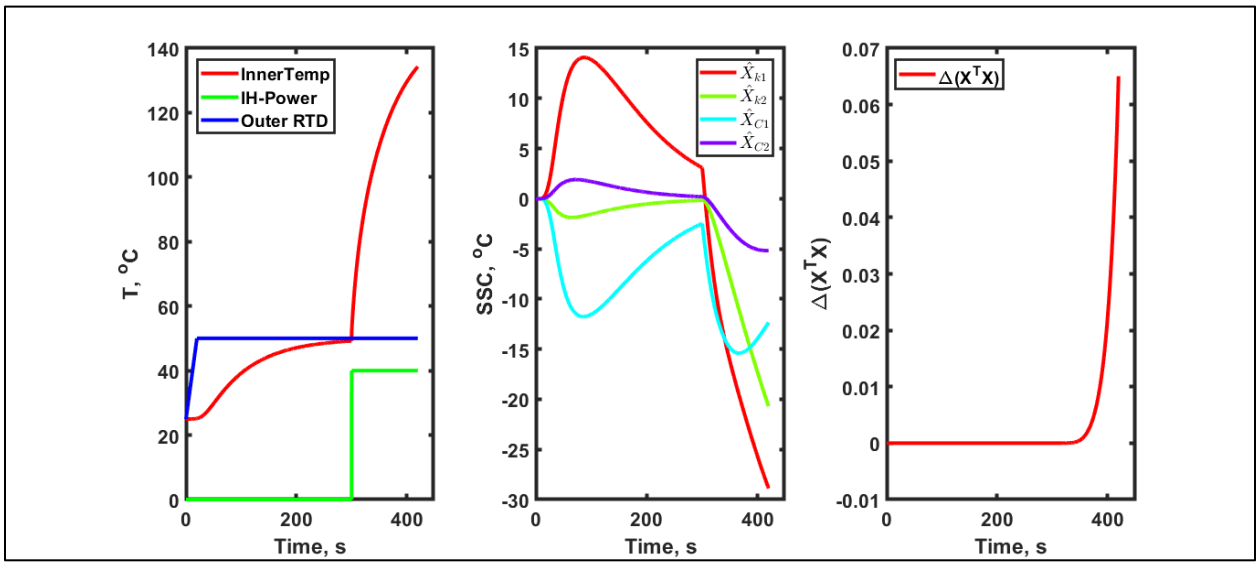

Figure 2.8: (a) Power and Temperature profile (b) SSCs for four parameters (c) Δ for a complementary experiment profile for k_h = 0.2 W/mK

3. *Combination Pulse of Power to Inner Heater, Outer RTD Maintained at Constant Temperature*

Another complementary experiment, with a different power function supplied to the inner heater, was analyzed (Fig. 2.9). The combination of exponential and sinusoidal functions as power input increases the Δ even further. The SSCs for each parameter increased. The inner RTD temperature became increasingly sensitive to changes in parameters. As a result, multiple parameters can be estimated accurately. From the data shown in Fig. 2.9, k_1 and C_1 can be estimated. Despite the large value of Δ, sensitivity of k_2 and C_2 is relatively small (less than 5 % of total inner RTD temperature rise) and as a result, k_2 and C_2 cannot be estimated. The k_h value of the inner heater used for this run was 0.01 W/mK. To check the influence of k_h on SSC of C_2, k_h was changed to 0.2 W/mK and the power function was changed accordingly. Results are shown in Fig. 2.10.

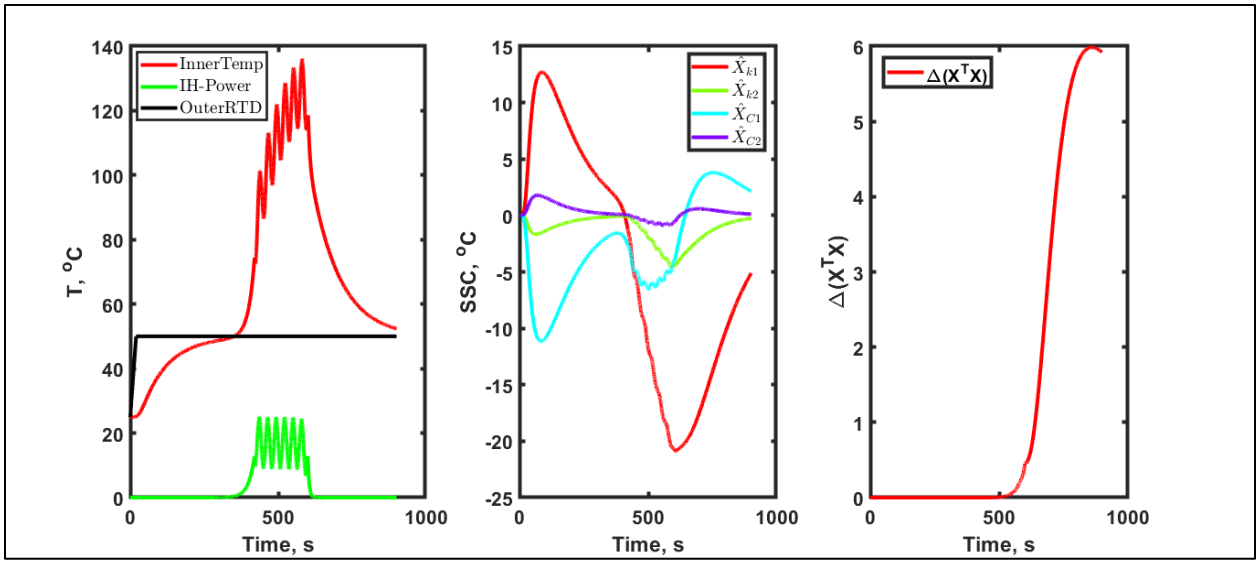

Figure 2.9: (a) Power and Temperature profile (b) SSCs for four parameters (c) Δ for combined pulse complementary experiment profile, k_h = 0.01 W/mK

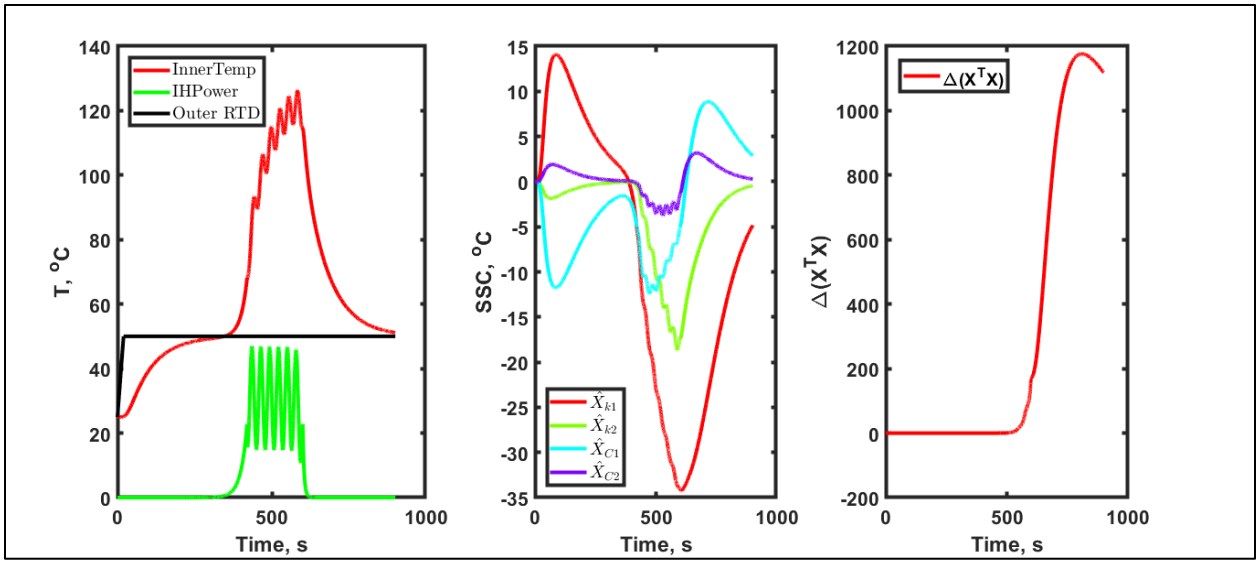

Figure 2.10 (a) Power and Temperature profile (b) SSCs for four parameters (c) Δ for combined pulse complementary experiment profile, k_h = 0.2 W/mK

Similar to case 2, changing thermal conductivity of the heater has a significant impact on the SSCs. In Fig. 2.10(b), it can be observed that the SSCs of k_2 and C_2 have increased. The SSC of k_2 increased by almost four times, making it well into the estimable range. The SSC of C_2 is about 5 % of the temperature rise, but higher than in Fig 2.9(b). This experiment can be optimized further.

The sinusoidal and exponential functions can be modified further to increase SSC of C_2. In addition, a heater with high thermal conductivity should be used.

2.4.2 Experimental Results

The design of experiment for validation was the same as the first complementary experiment described in 2.3.3 (Simulated profiles, case 2). The SSCs are plotted for k_1, k_2, C_1 and C_2 (Fig. 2.11). The heater properties used are: k_h = 0.01 W/mK and C_h = 2.4x10^6 J/m^{3}K. Similar to the simulated case, with the given heater properties, only k_1 and C_1 could be estimated. C_2 and k_2 were not estimable due to low SSCs (SSCs were less than 10% of total temperature rise). The SSCs for two parameter estimation (k_1 and C_1) are shown in Fig. 2.12.

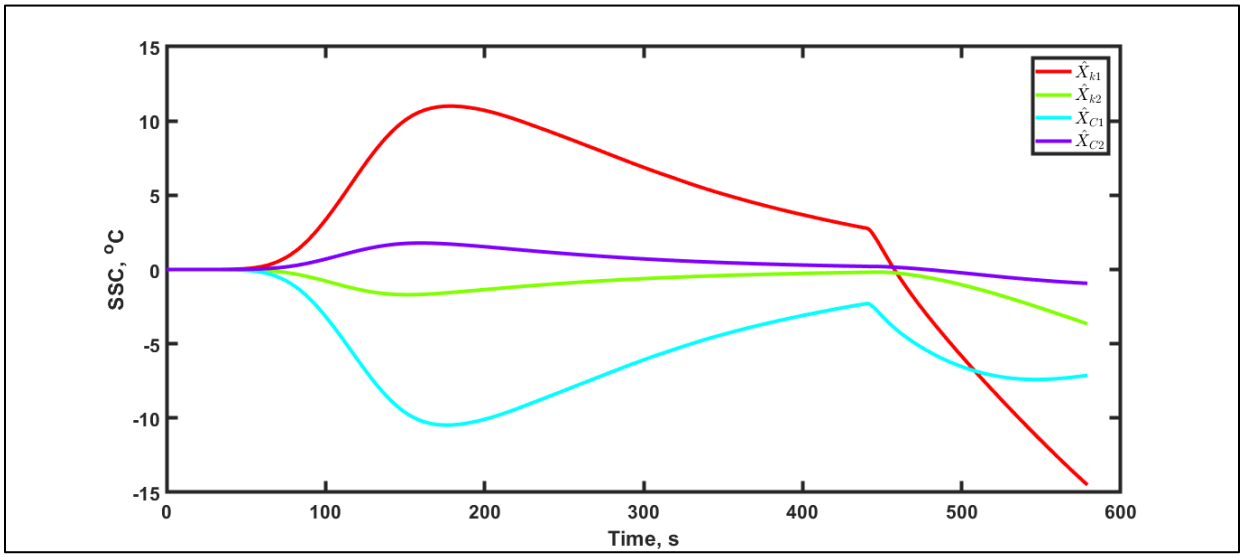

Figure 2.11 SSCs for four parameters for experimental data

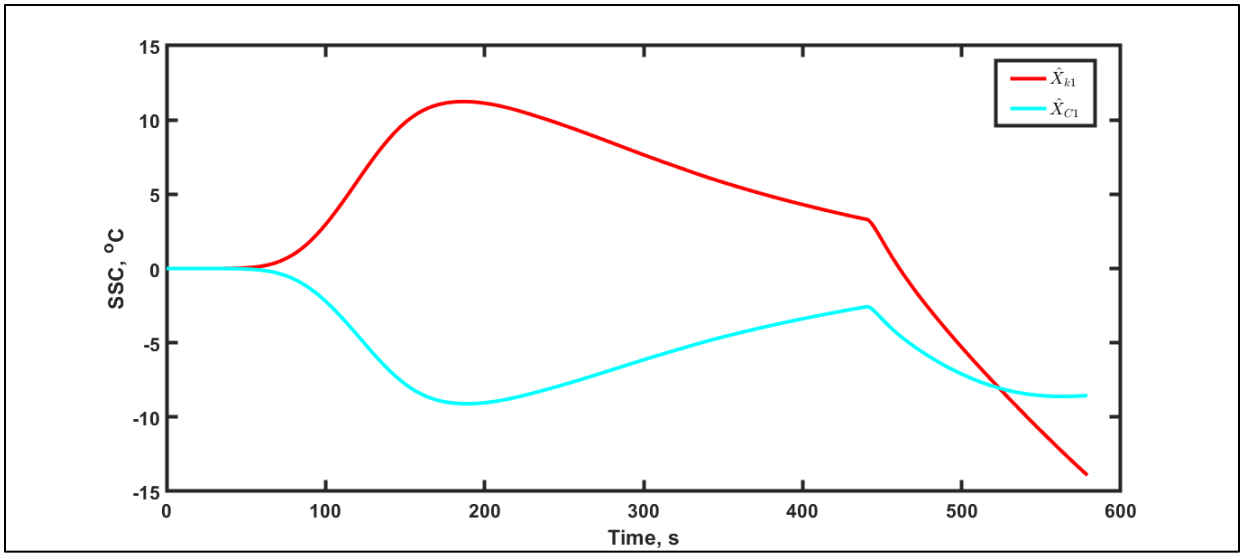

Figure 2.12 SSC for k_1 and C_1 for two parameter estimation from experimental data

Based on inference from the sensitivity analysis, k_1 and C_1 were sequentially estimated. Sequential estimation requires prior information (assumed initial values of parameters). The initial values used were: k_1 of sweet potato puree = 0.51 W/mK, C_1 of sweet potato puree = 3.612 x 10^6 J/m^3K, k_2 = 0.63 W/mK, C_2 = 3.870 x 10^6 J/m^3K.

Fig. 2.13 shows the trend of sequential estimation. The value of C_1 is scaled (divided by initial guess) to show both parameter estimates on the same plot. The trend becomes constant, indicating that the duration of the experiment was sufficiently long to estimate final values of parameters.

Fig. 2.14(a) shows the predicted and experimental inner RTD temperature after sequential estimation. Fig. 2.14(b) shows the residuals. The average estimated values are tabulated in table 2.1.

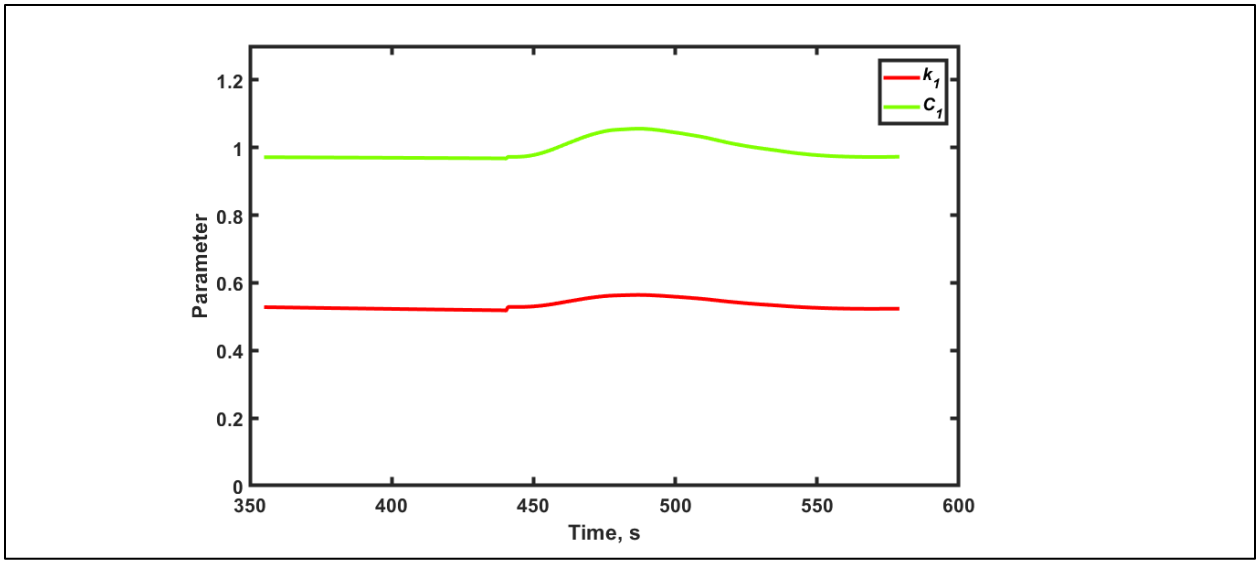

Figure 2.13 Sequential parameter estimates for k_1 and C_1. Values of C_1 are scaled (divided by initial guess value)

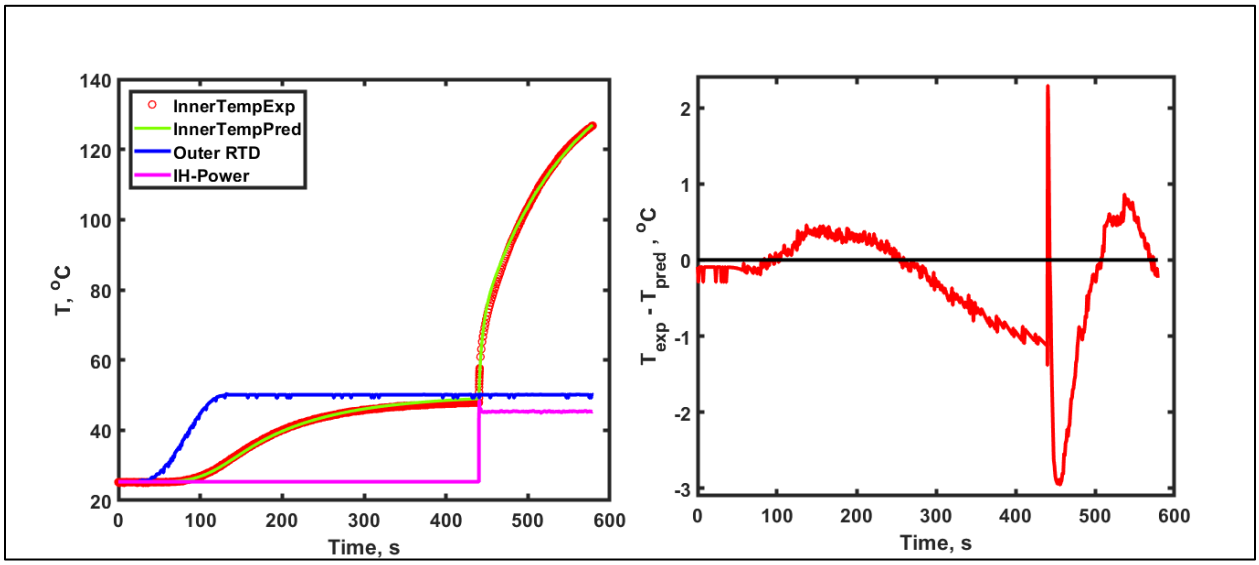

Figure 2.14 (a) Predicted vs experimental inner RTD temperature after estimation (b) Residuals

Table 2.1 Thermal properties of sweet potato puree

Thermal Property	Average Value from 5 tests	Standard Deviation	95% Confidence Interval	RMSE
k_1 (W/mK)	0.532	0.016	0.512 - 0.552	0.89
C_1 (J/m^{3}K)	3.562 x 10^6	1.24 x 10^5	3.408 x 10^6 - 3.716 x 10^6	

The estimated thermal properties closely matched literature values. The volumetric heat capacity closely matched published values (Fasina and Farkas, 2003). Thermal conductivity of sweet potato puree at 25°C calculated using the Choi-Okos predictive model was 0.535 W/mK. Thermal conductivity was measured at room temperature by using KD2 Pro (Table 2.2).

Table 2.2 Thermal properties of sweet potato puree at room temperature measured by KD2 Pro

Temperature, °C	Thermal Conductivity, (W/m°C)	Error	Mean k at 25.83°C = 0.539 W/m°C
25.82	0.540	0.0043	
25.83	0.537	0.0055	
25.84	0.541	0.0043	

The parameters estimated in the experimental runs are the same parameters that were deemed estimable by the result of the simulated runs. Thus, the use of sensitivity analysis saves time and resources. Simulating experiment designs in COMSOL and checking SSCs gives information about expected results and what improvements may be needed to optimize the experiment.

Complementary experiments are clearly more advantageous compared to non-complementary trials. Multiple parameters can be estimated from a single experiment. The number of experiments needed reduces significantly. Same experimental set-up can be used for a wide variety of materials, wide temperature range, to find temperature-dependent properties at multiple temperatures.

Thermal properties at high temperatures, k_2 and C_2, seem to be impacted in a more pronounced manner by the thermal conductivity of the inner heater (Fig. 2.7, 2.8, 2.9, 2.10). While k_2 has

become estimable, from the above results, SSC for C_2 is still not high enough to estimate it. The experiment can be optimized further to understand the relationship of C_2 with heater thermal properties. From an experimental perspective, using heaters with extremely high thermal conductivity would increase the probability of experimentally determining C_2. There may be other factors at play as well such as contact resistance between the layers, the thickness of layers in the thin film heater, convective currents in the sample tube, duration of the experiment etc. Further studies are needed to understand factors that need to be optimized to estimate C_2.

2.5 Conclusions

Complementary experiments were defined, designed and optimized to estimate multiple parameters from a single experiment. Temperature and power profiles were simulated in COMSOL. Scaled sensitivity coefficients were calculated for all parameters to check feasibility of estimation. Simulations and SSCs enabled designs of experiment in a resource efficient and cost-effective manner. Experimental data validated results of the simulated profiles. Experiments and simulations were used in conjunction with sequential parameter estimation to estimate thermal conductivity and volumetric heat capacity of sweet potato puree. The thermal conductivity and volumetric heat capacity of sweet potato puree at 25°C were found to be 0.532 W/mK and 3.562 x 10^6 J/kgK. The estimated values closely matched published values. Further studies are needed to identify all the factors affecting optimality of a complementary experiment to estimate multiple parameters.

2.6 References

Ahadi, M., Andisheh-Tadbir, M., Tam, M., & Bahrami, M. (2016). An improved transient plane source method for measuring thermal conductivity of thin films: Deconvoluting thermal contact resistance. *International Journal of Heat and Mass Transfer*, *96*, 371–380. https://doi.org/10.1016/j.ijheatmasstransfer.2016.01.037

Choi, Y., & Okos, M. (1986). Effects of temperature and composition on the thermal properties of foods. *Effects of Temperature and Composition on the Thermal Properties of Foods*, 93–101.

de Monte, F., Beck, J. V., & Amos, D. E. (2018). Optimum design of complementary transient experiments for estimating thermal properties. *Journal of Physics: Conference Series*, *1047*, 012002. https://doi.org/10.1088/1742-6596/1047/1/012002

E. Sweat, V., & G. Haugh, C. (1974). A Thermal Conductivity Probe for Small Food Samples. *Transactions of the ASAE*, *17*(1), 56–0058. https://doi.org/10.13031/2013.36786

Featherstone, S. (2012). A review of development in and challenges of thermal processing over the past 200years—A tribute to Nicolas Appert. *Food Research International*, *47*(2), 156–160. https://doi.org/10.1016/j.foodres.2011.04.034

Greiby, I., Mishra, D. K., & Dolan, K. D. (2014). Inverse method to sequentially estimate temperature-dependent thermal conductivity of cherry pomace during nonisothermal heating. *Journal of Food Engineering*, *127*, 16–23. https://doi.org/10.1016/j.jfoodeng.2013.10.039

Gustafsson, S. E. (1991). Transient plane source techniques for thermal conductivity and thermal diffusivity measurements of solid materials. *Review of Scientific Instruments*, *62*(3), 797–804. https://doi.org/10.1063/1.1142087

Huang, L., & Liu, L.-S. (2009). Simultaneous determination of thermal conductivity and thermal diffusivity of food and agricultural materials using a transient plane-source method. *Journal of Food Engineering*, *95*(1), 179–185. https://doi.org/10.1016/j.jfoodeng.2009.04.024

Mariani, V. C., Amarante, Á. C. C. D., & Coelho, L. D. S. (2009). Estimation of apparent thermal conductivity of carrot purée during freezing using inverse problem. *International Journal of Food Science & Technology*, *44*(7), 1292–1303. https://doi.org/10.1111/j.1365-2621.2009.01958.x

Martins, R. C., & Silva, C. L. M. (2004). Inverse problem methodology for thermal-physical properties estimation of frozen green beans. *Journal of Food Engineering*, *63*(4), 383–392. https://doi.org/10.1016/j.jfoodeng.2003.08.008

McMasters, R. L., de Monte, F., & Beck, J. V. (2017, July 9). Estimating Two Parameters From Two Complementary Transient Experiments. *HT2017*. https://doi.org/10.1115/HT2017-4702

Mishra, D. K., Dolan, K. D., Beck, J. V., & Ozadali, F. (2016). A novel instrument for rapid measurement of temperature-dependent thermal properties of conduction-heated food up to 140 °C. *Journal of Food Engineering*, *191*, 19–27. https://doi.org/10.1016/j.jfoodeng.2016.06.028

Mohamed, I. O. (2009). Simultaneous estimation of thermal conductivity and volumetric heat capacity for solid foods using sequential parameter estimation technique. *Food Research International*, *42*(2), 231–236. https://doi.org/10.1016/j.foodres.2008.11.002

Mohamed, I. O. (2010). Development of a simple and robust inverse method for determination of thermal diffusivity of solid foods. *Journal of Food Engineering*, *101*(1), 1–7. https://doi.org/10.1016/j.jfoodeng.2010.05.002

Monteau, J.-Y. (2008). Estimation of thermal conductivity of sandwich bread using an inverse method. *Journal of Food Engineering*, *85*(1), 132–140. https://doi.org/10.1016/j.jfoodeng.2007.04.034

Murakami, E. G., & Okos, M. R. (1989). Measurement and Prediction of Thermal Properties of Foods. In R. P. Singh & A. G. Medina (Eds.), *Food Properties and Computer-Aided Engineering of Food Processing Systems* (pp. 3–48). Springer Netherlands. https://doi.org/10.1007/978-94-009-2370-6_1

Muramatsu, Y., Greiby, I., Mishra, D. K., & Dolan, K. D. (2017). Rapid Inverse Method to Measure Thermal Diffusivity of Low-Moisture Foods. *Journal of Food Science*, *82*(2), 420–428. https://doi.org/10.1111/1750-3841.13563